Molecular Therapy
Nucleic Acids
Original Article

Effect of degeneration stage on non-viral tissue transfection of *rd10* retina *ex vivo*

Jiao Zhang,[1] Ziyu Bing,[1] Corinne Marie,[2,3] Zsuzsanna Izsvák,[4] Frank Müller,[5] Gabriele Thumann,[6,7] Peter Walter,[1] and Sandra Johnen[1]

[1]Department of Ophthalmology, Uniklinik RWTH Aachen, 52074 Aachen, Germany; [2]Université Paris Cité, CNRS, Inserm, UTCBS, 75006 Paris, France; [3]Chimie ParisTech, Université PSL, 75005 Paris, France; [4]Max Delbrück Center for Molecular Medicine in the Helmholtz Association, 13125 Berlin, Germany; [5]Institute of Biological Information Processing, Molecular and Cellular Physiology, IBI-1, Forschungszentrum Jülich GmbH, 52428 Jülich, Germany; [6]Department of Ophthalmology, University Hospitals of Geneva, 1205 Geneva, Switzerland; [7]Experimental Ophthalmology, University of Geneva, 1205 Geneva, Switzerland

Gene therapy has great potential for the treatment of inherited retinal diseases, as evidenced by the progress and ongoing research. Using the *Sleeping Beauty* (*SB*) transposon system, we developed a non-viral gene delivery system for electroporation-based transfection of *rd10* retinas *ex vivo*. *SB100X* transposase and *Venus* transposon plasmids were transfected at a ratio of 1:16 into *rd10* retinas of different ages and corresponding wild-type (WT) controls. Transfection efficiency was assessed by fluorescence microscopy and transfected cells were identified by immunohistochemistry. Retinal integrity and cell viability were assessed by FITC-dextran electroporation, histology, and apoptosis assay. The highest transfection efficiency was observed in degenerated stages P61 and older, with Müller cells being the only transfected cell type. A 31% reduction in transposon plasmid size resulted in a 1.5-fold increase in transfection efficiency. Integrity and morphology of degenerated retinas were preserved after electroporation-based plasmid transfer; the number of apoptotic cells in the inner nuclear layer (INL) was reduced by half compared to WT controls. We demonstrated that electroporation-based delivery of the *SB* transposon system resulted in efficient transfection of degenerated retinas. Our results are an important first step toward the combined use of retinal prostheses and gene therapy to improve the treatment of inherited retinal dystrophies.

INTRODUCTION

Retinitis pigmentosa (RP) is a major cause of blindness and visual impairment affecting more than 1.5 million people worldwide. It is an inherited disease characterized by progressive rod photoreceptor death followed by cone photoreceptor death.[1,2] Different therapeutic treatment strategies include gene therapy, cell therapy, optogenetics, and retinal prostheses.[3,4] As the disease progresses, RP leads to retinal remodeling, which is characterized by significant structural and functional changes in the retina. These changes can include synaptic reorganization, alterations in neuronal circuitry and changes in the release of neurotransmitters.[5,6] The *rd10* mouse, which is characterized by a missense mutation in the *Pde6b* gene encoding the β-subunit of phosphodiesterase 6, is an established model for RP due to the similarity of the progressive dystrophic phenotype observed in mouse and human photoreceptors.[7–10] In *rd10* mice, photoreceptor cell loss begins around postnatal day (P)18 in the central retina, extends to P20 in the peripheral retina, peaks around P25, and culminates in the absence of photoreceptors at P60.[10]

Gene therapy is a promising approach in which genes are introduced into cells to treat inherited or acquired diseases.[11] The eye is an ideal organ for gene therapy: it is easily accessible and can be easily monitored with non-invasive techniques; it is small and therefore requires low vector doses; it is immune-privileged and isolated due to different ocular barriers; and the fellow eye can serve as a control. Viral gene therapy is known to be highly effective and is already used in clinical practice for ocular diseases.[12] A well-known example is voretigene neparvovec-rzyl, approved in 2017, which delivers a functional copy of the *RPE65* gene via an adeno-associated viral (AAV) vector for the treatment of inherited retinal dystrophy (IRD) caused by a bi-allelic *RPE65* mutation.[13,14] However, transfer to any IRD is not trivial, as mutations in more than 250 genes have been described,[15] meaning that a separate vector must be produced for each affected gene. Although the success of AAV gene therapy is encouraging, there are limitations and challenges: ocular AAV gene therapy is associated with a cumulative incidence of serious adverse events of 8%, with inflammatory events often difficult to assess due to corticosteroid treatment[16]; AAVs have limited transgene packaging capacity, are difficult to produce, and are costly.[17] In contrast, non-viral vectors are characterized by low cytotoxicity and immunogenicity, high transgene capacity, ease of production and, in the case of the *Sleeping Beauty* (*SB*) transposon system, stable gene transfer delivery.

The *SB* transposon system is an integrating delivery system that results in efficient expression of transgenes in eukaryotic cells. It has

Received 24 October 2024; accepted 27 June 2025;
https://doi.org/10.1016/j.omtn.2025.102616.

Correspondence: Sandra Johnen, Department of Ophthalmology, University Hospital RWTH Aachen, Pauwelsstraße 30, 52074 Aachen, Germany.
E-mail: sjohnen@ukaachen.de

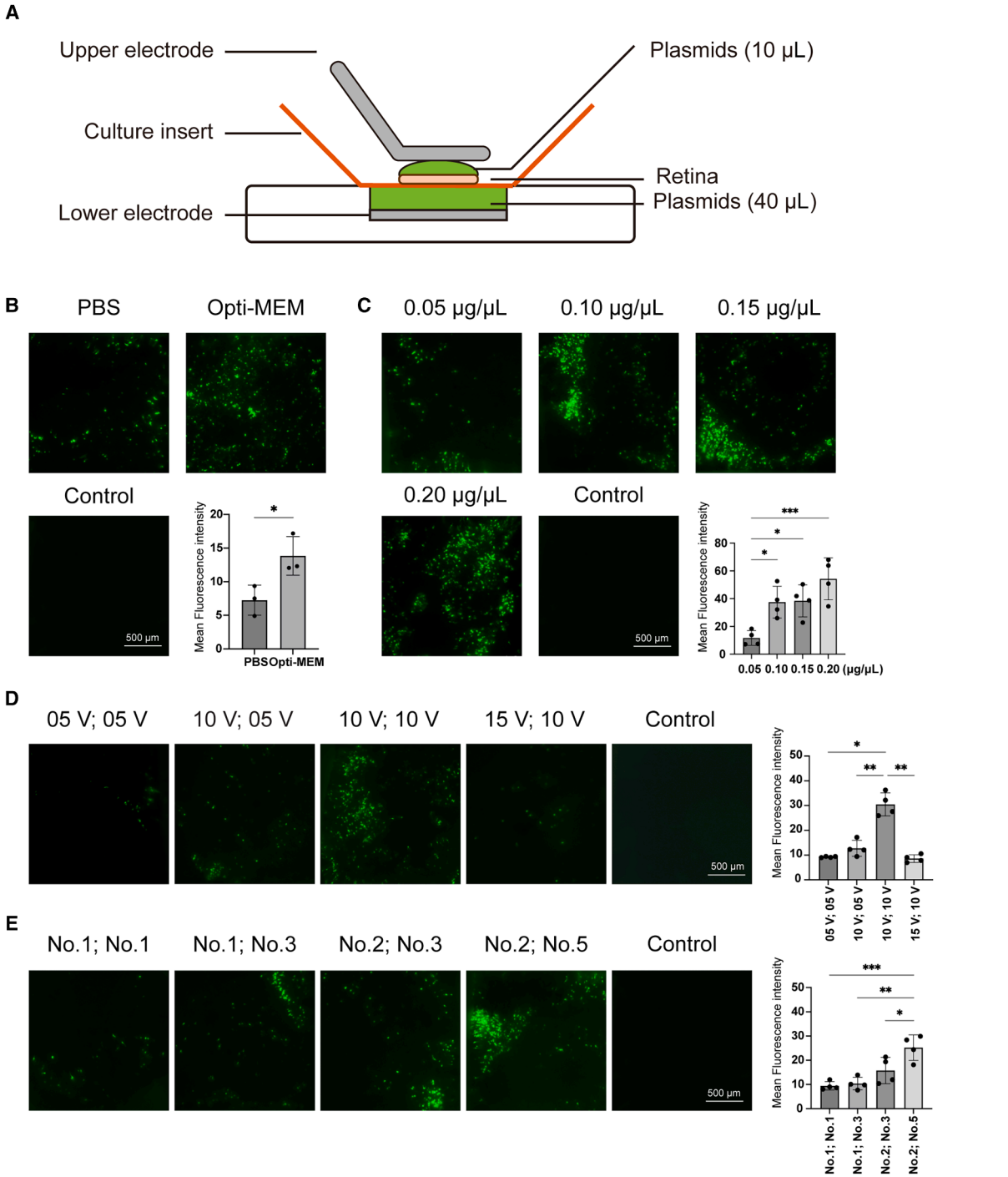

Figure 1. Optimization of various parameters for electroporation of 3-month-old *rd10* retinas using the *SB100X* transposon system

(A) Illustration of the *ex vivo* retinal electroporation. The retina (orange) was mounted on the filter of a culture insert (red) and positioned between the upper and lower electrodes (gray). The well of the lower electrode was filled with 40 µL of electroporation buffer (green) containing the plasmid mixture, and an additional 10 µL of the plasmid mixture was applied directly onto the retinal tissue. (B) Optimization of electroporation buffer. Flat-mounted retinas were transfected with PBS and Opti-MEM electroporation buffer containing 0.10 µg/µL of a plasmid mixture composed of *SB100X* transposase plasmid and pT2-CAGGS-*Venus* transposon plasmid at a ratio 1:16. The bar graph shows that the mean fluorescence intensity of transfected cells was significantly higher with Opti-MEM buffer than with PBS buffer ($n = 3$, $^*p = 0.0352$, using unpaired two-tailed t test). (C) Optimization of plasmid concentration. Flat-mounted retinas transfected with increasing concentrations of 0.05, 0.10, 0.15, and 0.20 µg/µL of the purified

(legend continued on next page)

been used in basic research in the field of gene and cell therapy, in numerous preclinical studies, and also in clinical trials, as described in various review articles.[18–20] The *SB* transposon system consists of a transposon DNA sequence and a transposase enzyme whose genetic information is encoded on a separate plasmid. The transposon is characterized by inverted terminal repeats (ITRs), which contain binding sites for the transposase, allowing it to catalyze the transposition reaction and incorporate specific genetic information, such as genes, into the target genome.[18,21,22] This *SB*-catalyzed genomic integration is stable and ensures long-term expression of the transgene. The close-to-random integration profile at the genomic level, which significantly reduces the risk of potential insertional mutagenesis, makes the *SB* transposon system an effective and safe technique for human gene therapy.[23–25] In previous studies, we have shown that the gene encoding pigment epithelium-derived factor (PEDF) can be successfully introduced into ARPE-19 cell suspensions as well as primary retinal and iris pigment epithelial cells by electroporation.[26–28] PEDF is a naturally occurring protein in the eye, and it was selected for its ability to suppress neovascularization and its neurotrophic properties to protect cells and block neuronal degeneration. Expression and secretion of integrated PEDF were detected for up to 16 months. Notably, this technique did not impact the cobblestone morphology of the primary pigment epithelial cells. Using the antibiotic-free pFAR4 miniplasmid vector in combination with the *SB* transposon system, a further more than 2-fold increase in recombinant PEDF secretion was observed.[29] The overall goal is to use *ex-vivo* transfected cells as autologous drug delivery system that are retransplanted into the patient to allow secretion of a comprehensive therapeutic protein at the graft site. Subretinal transplantation of these *SB*-PEDF-transfected cells could provide a longer-lasting alternative to the current treatment of neovascular age-related macular degeneration with repeated intravitreal injections of anti-VEGF antibodies.[30]

The retina has a structured lamination and complex intercellular communication that enables it to respond effectively to injury and maintain homeostasis.[31] *Ex-vivo* retinal explants preserve this tissue complexity and physiological properties and reflect phenotypes associated with aging at different stages in mice, making them an ideal model to study the progression of retinal degenerative diseases.[32–34] We have extended our transfection protocols to *ex-vivo* retinal tissue to study the spatiotemporal dynamics of transfected cells at different stages of retinal degeneration.

In this work, we used *SB100X* transposon-based gene transfer by electroporation to achieve efficient transfection of whole retinal tissue while minimizing damage. In addition, we investigated the effects of this method on transfection efficiency, transfected cell types, and cell survival after electroporation and cultivation. Understanding the different parameters of transgene integration at different stages of degenerative retinal remodeling is crucial for the development of targeted therapeutic interventions.

RESULTS

Establishment of electroporation-based *ex-vivo* transfection of *rd10* retinas

Our aim was to establish and explore the optimal parameters for electroporation of degenerated retina *ex vivo*. Different electrical conditions were systematically investigated in 3-month-old (3M) *rd10* mice whose retinas had already degenerated. The electroporation system for mouse retinal tissue includes a flat upper electrode held by a micromanipulator and a lower electrode chamber filled with electroporation buffer. Retinal tissue was mounted on the culture insert with the ganglion cell layer (GCL) facing up and then placed on the bottom electrode. Retinas were transfected with a *SB100X* transposase and pT2-CAGGS-*Venus* transposon plasmid mixture at a ratio of 1:16 and a total plasmid concentration of 0.1 μg/μL. Plasmid mixtures (10 and 40 μL) were applied separately to the retina and to the well of the electroporation dish (Figure 1A). Negative controls were performed with adding the plasmid mixture but without application of electroporation pulses. After electroporation, retinas were cultivated and *Venus* expression was analyzed after 24 h of incubation by fluorescence microscopy.

As the NEPA21 electroporator does not require the use of a specific electroporation buffer, phosphate-buffered saline (PBS) and Opti-MEM buffer were analyzed. The fluorescence intensity value in flat-mounted retinal tissue was significantly higher after transfection with Opti-MEM buffer than after transfection with PBS buffer (13.85 ± 2.88 vs. 7.26 ± 2.24; Figure 1B). Plasmid concentrations of 0.05–0.20 μg/μL were used for electroporation. A clearly pronounced *Venus* expression distributed over the whole-mounted retina was shown for 0.10, 0.15, and 0.20 μg/μL plasmid DNA. However, no significant difference in transfection efficiency was observed between these three concentrations (37.49 ± 11.47 for 0.10 μg/μL, 38.44 ± 11.55 for 0.15 μg/μL, and 54.31 ± 15.12 for 0.20 μg/μL; Figure 1C). Given the need to minimize the amount of exogenously applied DNA to reduce potential side effects, the use of 0.1 μg/μL of purified plasmid mixture diluted in Opti-MEM electroporation buffer was established as the plasmid concentration for further experiments.

plasmid mixture showed increasing transfection efficiencies. The bar graph shows a significant increase in the mean fluorescence intensity of transfected cells when the plasmid concentration exceeded 0.10 μg/μL ($n = 4$, $^{*}p < 0.05$, and $^{***}p = 0.0010$, using one-way ANOVA test with Tukey's multiple comparisons test). (D) Optimization of electrical pulse parameters. Flat-mounted retinas were transfected with different settings for the poring and transfer pulse. The bar graph shows that the ideal voltage settings were 10 V for the poring pulse and 10 V for the transfer pulse ($n = 4$, $^{*}p = 0.0105$, and $^{**}p < 0.01$, using Brown-Forsythe and Welch ANOVA tests with Dunnett's T3 multiple comparisons test). (E) Optimization of the number of electroporation pulses. Flat-mounted retinas were transfected with different numbers of poring and transfer pulses. The bar graph shows that the ideal number of pulses was 2 poring pulses and 5 transfer pulses ($n = 4$, $^{*}p = 0.0296$, $^{**}p = 0.0012$, and $^{***}p = 0.0007$, using one-way ANOVA test with Tukey's multiple comparisons test). Scale bars, 500 μm.

With regard to the electroporation program, the electrical voltage and the number of pulses were examined. We found that lower voltages (Figure 1D) and lower number of pulses (Figure 1E) were associated with low transfection efficiency. Therefore, the optimal parameters were set as follows: 10 V, 2 pulses for the poring pulse voltage and 10 V, 5 pulses for the transfer pulse voltage. The parameters pulse length, pulse interval, pulse decay rate, and pulse polarity were set according to the manufacturer's recommendations (Figure S1). In summary, the following electroporation parameters were defined for further experiments: 10 V pulse voltage, 5 ms pulse length, 50 ms pulse interval, 2 pulses, 10% pulse decay rate, and bipolar pulse polarity for the poring pulse; 10 V pulse voltage, 50 ms pulse length, 50 ms pulse interval, 5 pulses, 40% pulse decay rate, and bipolar pulse polarity for the transfer pulse.

To investigate the impact of *SB100X* transposase on the transfection efficiency, flat-mounted *rd10* retinas were electroporated with either the transposon plasmid pT2-CAGGS-*Venus* alone or in combination with the *SB100X* transposase plasmid, followed by 5-day cultivation (Figures S2A and S2B). Daily assessment of transfection efficiency revealed that *SB100X* co-delivery significantly enhanced transgene expression compared to transposon-only controls (20.30 ± 5.45 vs. 11.65 ± 2.64; Figure S2C). Furthermore, both groups exhibited a time-dependent increase in gene expression levels.

Identification of Müller cells as the transfected cell type

To identify the cell types transfected by electroporation with the *SB* transposon system, we performed immunofluorescence staining with different retinal cell type markers on retinas of 3-month-old *rd10* mice. After staining, we examined the intensity of co-localization between pT2-CAGGS-*Venus*-labeled transfected cells and the different retinal cell populations Müller cells, amacrine cells, and horizontal cells. Our results showed that cells transfected with pT2-CAGGS-*Venus* traversed all retinal layers, from the inner nuclear layer (INL) to the GCL. Assessment of fluorescence intensity showed a clear preference for co-localization between transfected cells and Müller cells (Figure 2A), as opposed to amacrine and horizontal cells (Figures 2B and 2C). Based on the morphology of the transfected cells and immunofluorescence co-localization, we were able to identify Müller cells as the only cell type that was transfected.

Transfection efficiency at different stages of degeneration in the *rd10* retina

To investigate the applicability of the optimized electroporation conditions at different stages of retinal degeneration, we performed electroporation at different characteristic *rd10* symptom stages. Notably, effective transfection was observed in *rd10* retinas from P61 onwards. The most effective transfection for P61, 3M, and 6-month-old (6M) *rd10* retinas was achieved with a poring pulse voltage and a transfer pulse voltage of 10 V each, with no significant difference between P61 (43.15 ± 13.13), 3M (33.35 ± 10.42), and 6M *rd10* retinas (45.91 ± 11.72; Figures 3A and 3B). In contrast, the introduction of genetic material into the retina of P16 and P25 *rd10* mice was associated with considerable difficulties at all voltages tested (Figure 3A). These results highlight the age- and degeneration-related differences in transfection efficiency of the *rd10* retina. It should be noted that age-matched wild-type (WT) retinas could not be successfully transfected under the same electroporation conditions (data not shown).

Cell membrane integrity after electroporation-based transfection

Stable electroporation-based transgene expression requires the successful uptake of foreign nucleic acids into the cell cytoplasm, their transport into the nucleus, and integration into the host genome. Our preliminary experiments showed that very little or no successful transfection using the *SB100X* system was observed in young *rd10* retinas (Figure 3A). To investigate whether the integrity of the cell membrane is altered in these retinas, FD4 was introduced into retinal tissue from *rd10* and WT mice of different ages (P16 - 6M). It should be noted that electroporation of P16 WT retinas could not be performed because mice of this age were not available from commercial sources. Immediately after electroporation, the flat-mounted retinas were examined by confocal microscopy. The control group was created by incubating retinas with FD4 for the same duration as the electroporation procedure, but without electroporation. No positive FD4-transfected cells were detected in the control groups (data not shown). The electroporated cells in the *rd10* retinas of all ages showed clear green fluorescence, indicating the introduction of the FITC-dextran dye into the cells. A clear cell shape was seen in the magnified images, indicating a reversible recovery of the cell membrane after electroporation in both *rd10* and WT retinas (Figure 4A). In contrast to electroporation-based transposon plasmid uptake, FD4 was successfully detected in the cells of young *rd10* (P16, P25) retinas, demonstrating the correct definition of electroporation parameters and procedures (Figure 4B). Furthermore, the FD4 transfection efficiency did not differ significantly between different stages of *rd10* and WT retinas (Figure 4C).

Structure of the electroporated and cultivated *rd10* retina

To assess the effects of transfection on the structural integrity of the adult retina, histological examination with hematoxylin and eosin (H&E) staining was performed on 3-month-old *rd10* retinas characterized by photoreceptor degeneration; age-matched, non-degenerated WT retinas were used for comparison. Six different conditions were evaluated, roughly divided into two groups: without cultivation and with cultivation. In each group, the retinal tissue was subjected to electroporation with or without the addition of the plasmid-based transposon system. The negative control included neither electroporation nor addition of the transposon plasmids. H&E staining showed that degenerated *rd10* retinas retained their structure after electroporation and cultivation. The total thickness of the *rd10* retina was in the range of 100.80 ± 0.79 μm and showed no significant differences due to the transfection and cultivation procedures (Figures 5A [top row] and 5B). In the group of non-cultivated WT retinas, clearly distinguishable retinal layers were detected and there were no significant changes due to the electroporation and transfection procedures, as shown by histological staining and quantification of retinal thickness. However, after 24 h of cultivation, loosening of

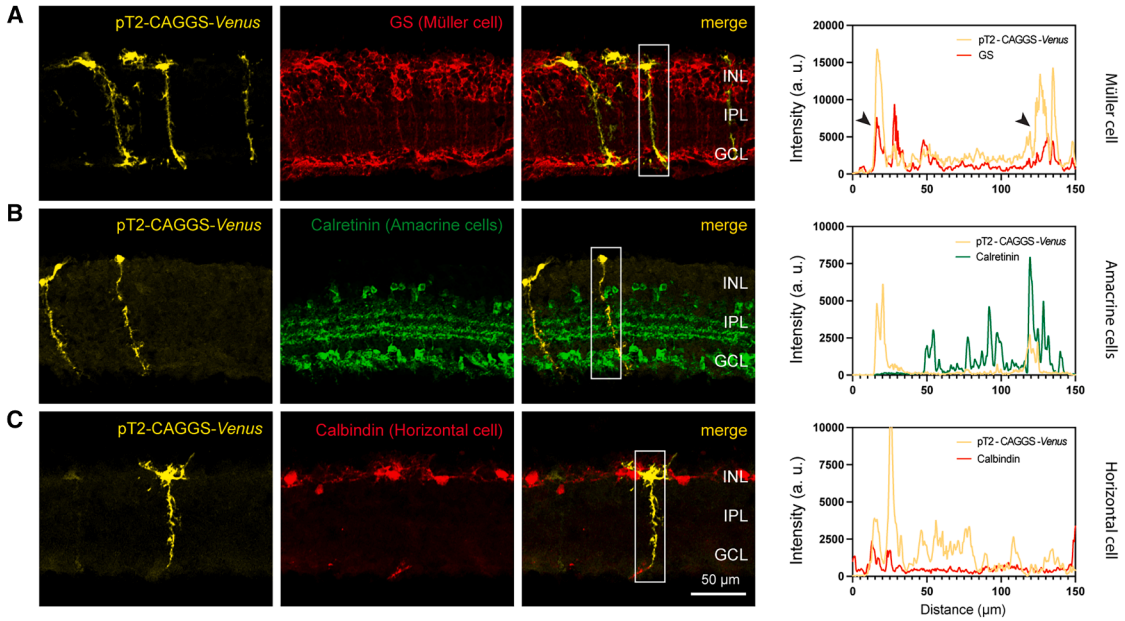

Figure 2. Transfected cell type in the retina of 3-month-old *rd10* mice

(A) Processes of pT2-CAGGS-*Venus* transfected yellow fluorescent cells traversed all retinal layers from the INL to the GCL. Anti-glutamine synthetase (GS)-stained Müller cells red. The fluorescence intensity diagram shows that pT2-CAGGS-*Venus* transfected cells had comparable fluorescence intensity characteristics to Müller cells labeled with anti-GS antibody. (B) Anti-calretinin labeled a representative subpopulation of amacrine cells in green. No obvious co-localization was observed between pT2-CAGGS-*Venus*-labeled transfected cells and anti-calretinin. (C) Anti-calbindin labeled horizontal cells red. No co-localization was observed between pT2-CAGGS-*Venus*-labeled transfected cells and anti-calbindin. INL, inner nuclear layer; IPL, inner plexiform layer; GCL, ganglion cell layer. Scale bars, 50 μm.

the retinal layers caused by electroporation and plasmid transfection was significantly greater than in the non-cultivated groups. This effect was observed in both inner and whole WT retinas (Figures 5A [bottom row] and 5C).

Influence of electroporation and cultivation on the survival of retinal cells

A cell apoptosis assay was performed on retinas of 3-month-old *rd10* mice and age-matched WT mice. The experimental setup included the same conditions as described before. In the group of non-cultivated *rd10* retinas, the transfection process generated a limited number of apoptotic cells compared to the corresponding control groups (Figures 6A [top row, left] and 6B). However, cultivation resulted in a significant increase in the number of apoptotic cells/field of view compared to the corresponding non-cultivated *rd10* retinas (82.33 ± 12.58 vs. 1 ± 1.73 cells in INL; 24.67 ± 8.62 vs. 0 cells in GCL). Furthermore, the electroporation procedure itself and the transfection of the transposon plasmid led to a significant increase in cell apoptosis in cultivated *rd10* retinas (110.3 ± 6.03 and 142.30 ± 8.02 cells in INL; 46.33 ± 10.69 and 50.67 ± 7.51 cells in GCL; Figures 6A [top row, right] and 6B). In the non-cultivated WT retinas, a significant increase in the number of apoptotic cells was observed after transposon plasmid transfection (42.67 ± 13.05 cells in INL; 14.67 ± 5.69 cells in GCL; Figures 6A [bottom row, left] and 6C). Similar to *rd10* retinas, a significant increase in apoptotic cells was observed throughout the WT retinas after 24 h of cultivation; however, the additional effect of electroporation and transposon plasmid delivery on apoptosis as observed in *rd10* retinas was not detectable (Figures 6A [bottom row, right] and 6C).

Effect of transposon plasmid size on transfection efficiency in *rd10* retinas

To investigate the influence of vector size on electroporation efficiency, we compared the introduction of transposon plasmids of different sizes: pT2-CAGGS-*Venus* (6,132 bps) and pFAR4-ITRs-CAGGS-*Venus* (4,227 bps). These two transposon plasmids were transfected at a concentration of 0.1 μg/μL into *rd10* retinas at different stages of degeneration. After 24 h of cultivation, the expression of the *Venus* reporter gene in flat-mounted retinas was analyzed by fluorescence microscopy.

Our results showed successful transfection of pT2-CAGGS-*Venus* in *rd10* mice from P61 onwards. Notably, no transfected cells were detected at the earlier stages of P16 and P25. Using pFAR4-ITRs-CAGGS-*Venus*, expression was seen at all developmental stages, but with significantly lower efficiency at P16 and P25 (Figure 7A). Transfection efficiency of the different transposon plasmids was analyzed quantitatively by measuring the mean fluorescence intensity. In young *rd10* retinas (P16 and P25), the fluorescence intensity using pFAR4-ITRs-CAGGS-*Venus* plasmid was 11.09 ± 1.37 at P16 and 10.56 ± 3.19 at P25 (Figure 7B [top]). At P61, a significant increase in fluorescence intensity was observed with

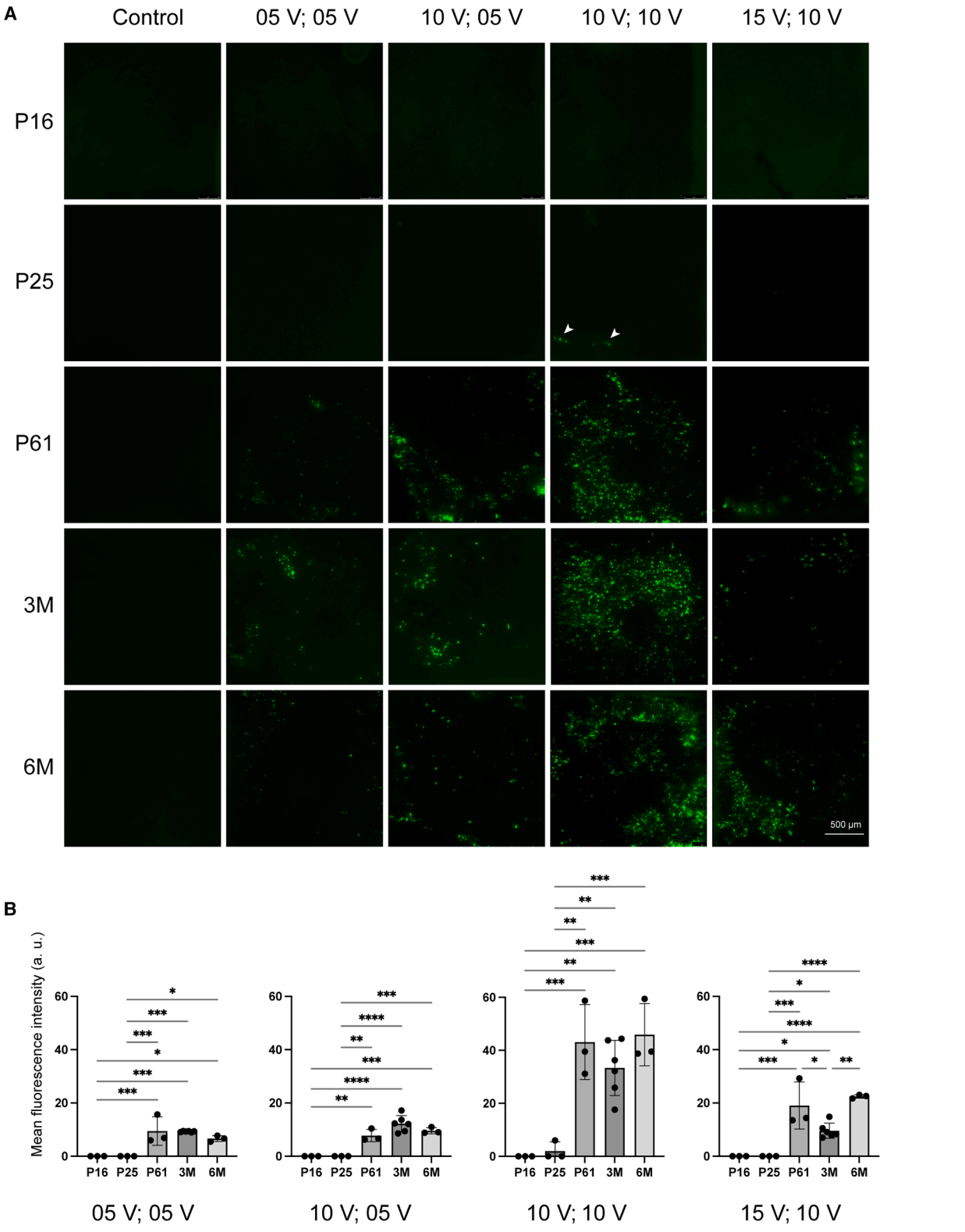

(legend on next page)

pFAR4-ITRs-CAGGS-*Venus* (64.04 ± 6.16) compared to pT2-CAGGS-*Venus* (44.35 ± 6.89). This effect was also observed in 3M and 6M *rd10* retinas (62.07 ± 3.54 vs. 42.62 ± 6.58 and 64.61 ± 3.37 vs. 36.35 ± 4.87, respectively; Figure 7B [bottom]).

To investigate the low transgene expression in the younger *rd10* retinas P16 and P25, we analyzed the expression of glial fibrillary acidic protein (GFAP), an inflammatory marker, in pFAR4-ITRs-CAGGS-*Venus* transfected retinas compared to non-transfected and adult *rd10* retinas. Three different experimental conditions were evaluated: no transfection and no cultivation (control), cultivation without transfection, and cultivation after transfection. In P16 *rd10* control retinas, GFAP expression was restricted to astrocytes in the GCL. After transfection and cultivation, Müller cells became slightly GFAP-positive. Clear morphological damage was visible (Figure S3A), which was also observed in transfected WT retinas (Figures 5 and 6). In P25 *rd10* retinas, high GFAP expression was observed in all Müller cells regardless of the experimental conditions (Figure S3B). In adult *rd10* retinas (P61 - 6M), GFAP expression in Müller cells did not increase significantly after transfection and cultivation compared to the corresponding control groups (Figures S3C–S3E).

Analysis of the transfected cell type using different transposon vector sizes

It is known that a reduction in plasmid size leads to an increase in transfection efficiency. Therefore, we further investigated the possible effect of plasmid size on the type of cell transfected. P61, 3M, and 6M old *rd10* retinas were transfected with the plasmids pT2-CAGGS-*Venus* and pFAR4-ITRs-CAGGS-*Venus*. Transfected cells were identified using retinal cell markers for Müller cells, amacrine cells, and horizontal cells in cross-sections of *rd10* retinas, followed by co-localization analysis. In P61 *rd10* retinas, yellow fluorescent transfected cells crossed all retinal layers, with the pFAR4-ITRs-CAGGS-*Venus* transfected cells being particularly prominent. Nevertheless, co-localization analysis showed a consistent dominance of Müller cells as transfected cells, independent of transposon plasmid size (Figure 8A). In 3M and 6M old *rd10* retinas, consistent results were observed, with the highest population of transfected cells in retinas transfected with the pFAR4-ITRs-CAGGS-*Venus* plasmid. Again, the reduction in plasmid size did not result in transfection of any retinal cell type other than Müller cells (Figures 8B and 8C). Quantification of Venus protein expression showed that electroporation with the pFAR4-ITRs-CAGGS-*Venus* plasmid resulted in a significantly higher transfection efficiency than electroporation with the pT2-CAGGS-*Venus* plasmid (Figure 8D), which is consistent with the results of transfection efficiency analysis of flat-mounted retinas (Figure 7).

DISCUSSION

In this study, we established an electroporation-based non-viral *ex-vivo* gene delivery method using the *SB* transposon system in *rd10* retinal tissue and analyzed the effects of degeneration and remodeling on transfection efficiency.

First, we optimized various settings for successful and efficient transgene delivery into *rd10* retinas *ex vivo*, including the choice of electroporation device, electroporation buffer, plasmid concentration, and electroporation parameters. Since the overall goal is to establish a gene therapy approach for degenerative retinal diseases, we performed these optimization experiments with degenerated retinas of 3-month-old *rd10* mice. A new version of the NEPA21 type II electroporator was used, which adjusts and monitors the input and output parameters of electroporation, allowing accurate optimization and verification of the actual electroporation parameters applied. Previous studies demonstrated a direct correlation between electric field intensity and transfection efficiency,[35,36] underscoring the importance of optimizing electrical parameters to achieve effective transfection with minimal cell damage. Opti-MEM buffer was chosen as the electroporation buffer as it showed higher transfection efficiency compared to the conventional electroporation PBS buffer.[37–39] In addition, previous studies showed that Opti-MEM buffer was able to improve cell viability during electroporation.[40,41] With 0.1 μg/μL of plasmid DNA per electroporation, a concentration was chosen that provided a significantly increased transfection efficiency. Although higher plasmid concentrations resulted in even better transfection efficiencies in some cases, we chose this concentration because previous studies showed that plasmid concentration is a critical parameter for electroporation, as it is inversely proportional to cell viability.[40]

To identify the cell types transfected in the degenerated *rd10* retinas by this method, we performed immunofluorescence staining with retinal cell-specific markers and analyzed the co-localization with the *Venus*-transfected cells. Our results showed that *Venus*-labeled cells traversed the degenerated *rd10* retinal layers vertically from the INL to the GCL. Detailed analysis of fluorescence intensity and cell morphology showed a clear preference for Müller cell transfection, consistent with previous studies.[39,42] In response to retinal degeneration, Müller cells undergo reactive gliosis with hypertrophy,

Figure 3. Transfection efficiency and optimization of electroporation parameters of *rd10* retinas at different ages

(A) Flat-mounted *rd10* retinas at different stages of degeneration were electroporated with 0.10 μg/μL *SB100X* transposase plasmid and pT2-CAGGS-*Venus* transposon plasmid mixture (ratio 1:16) using different poring pulse and transfer pulse voltages. The control group was treated identically but without the use of electroporation parameters (data not shown). No cells were transfected in P16 *rd10* retinas. Few cells were transfected in P25 *rd10* retinas at a poring pulse of 10 V and a transfer pulse of 10 V (arrowheads). The P61, 3M, and 6M retinas were successfully transfected with different poring and transfer pulses. At 10 V for the poring pulse and 10 V for the transfer pulse, adult *rd10* retinas showed higher transfection efficiency than at other voltage settings. (B) The graphs show the mean fluorescence intensity of P16, P25, P61, 3M, and 6M *rd10* retinas using different poring and transfer pulses. Each group consisted of a minimum of 3 retinas. $^{*}p < 0.05$, $^{**}p < 0.01$, $^{***}p < 0.001$, and $^{****}p < 0.0001$, using one-way ANOVA with Tukey's multiple comparisons test. Scale bars, 500 μm.

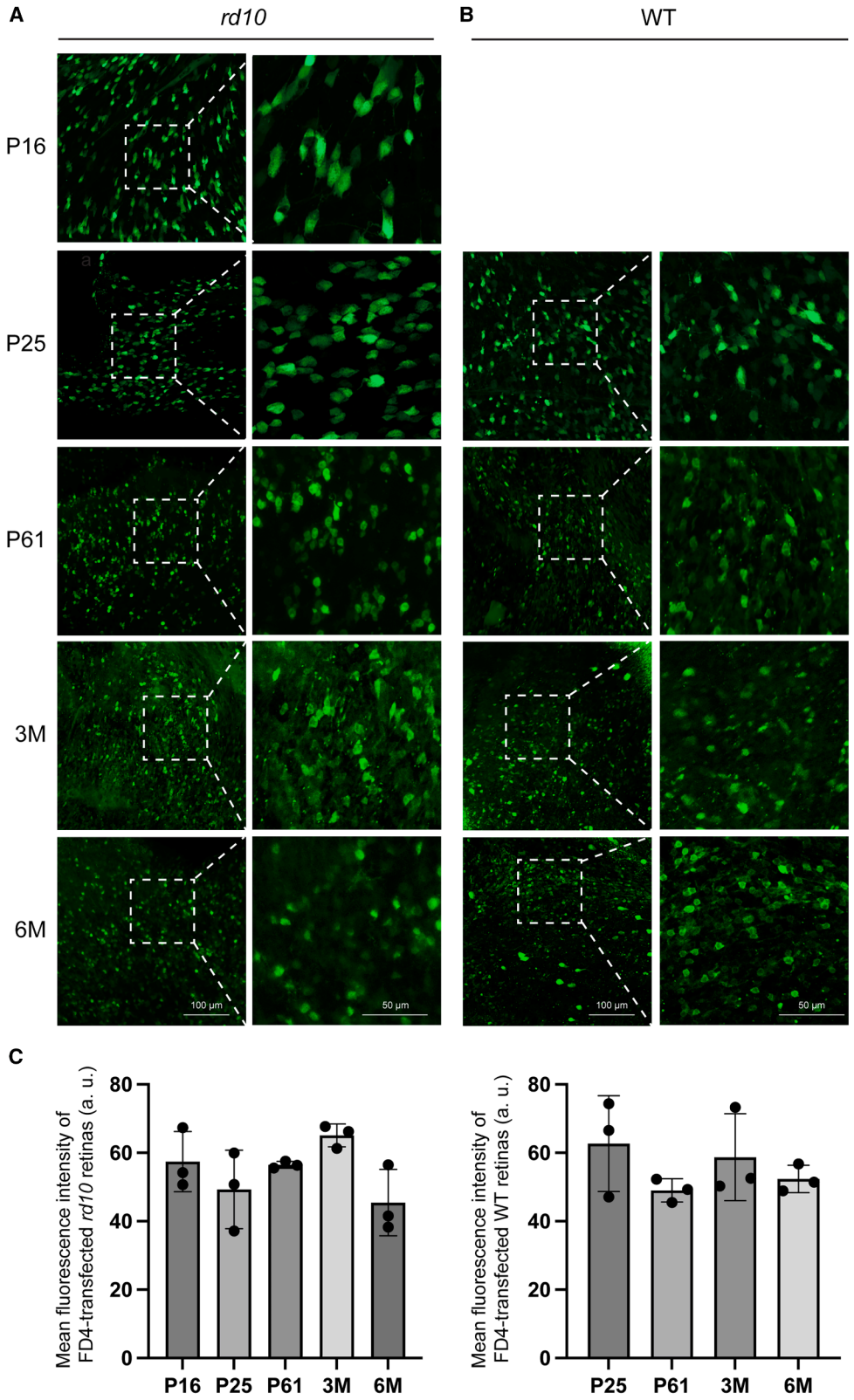

(legend on next page)

proliferation, translocation, and glial scarring,[43–46] which may make them more amenable to transfection agents. In addition, the other cell types are located in the glial shadow of the Müller cell endfeet and are therefore less likely to come into contact with the electrodes or lie outside the applied electrical field. Matsuda and Cepko showed that the developmental stage of the retina influences the transfection capacity. Retinas from WT rats electroporated *in vivo* at P0 showed GFP-positive rod photoreceptors, bipolar cells, Müller cells and amacrine cells as the animals aged. *Ex-vivo* electroporation of WT mouse retinal explants showed strong GFP fluorescence over large areas of the P0 retina, whereas few GFP-positive cells were detected in the adult retina.[42] In contrast, other studies showed that ganglion cells in adult mice and rat retinas can be transfected both *ex vivo* and *in vivo* by electroporation.[39,47]

Comparison of transfection efficiency at different ages of *rd10* retinas showed a correlation between the progression of degeneration and the transfectability of retinal cells with our non-viral gene delivery method. Adult P61, 3M, and 6M old *rd10* retinas showed effective transfection, probably due to glial scarring, whereas younger *rd10* (P16 and P25) retinas showed significant transfection resistance under identical experimental conditions. The experiments were also performed with WT retinas (data not shown). The parameters established for degenerated *rd10* retinas did not result in successful plasmid transfection in non-degenerated WT retinas, which appeared to be a robust barrier to plasmid DNA uptake.

We used dextran dye to evaluate the electroporation procedure and integrity of retinal cell membranes, as it is non-permeant to cell membranes and requires electroporation for cellular entry.[48] Our negative control group, in which the retinas were incubated in FD4 without electroporation, showed no fluorescence (data not shown). In contrast, the successful introduction of FD4 into cells of all ages of *rd10* and WT retinas after electroporation indicates that the electroporation parameters and procedures we established were correct and allowed effective uptake of molecules into the cell cytoplasm. Furthermore, the intact cell morphology without FD4 leakage suggests that electroporation-induced pore formation in the cell membrane is transient and reversible. However, successful electroporation-based FD4 delivery is not synonymous with successful DNA transfection as it is a complex process that requires DNA to be transcribed and translated once it has entered the cytoplasm or cell nucleus.[49]

Histological analysis and cell apoptosis assay showed that both the application of electrical pulses and plasmid transfection had minimal effects on morphology and cell survival in degenerated *rd10* retinas. In contrast, significant damage and cell death were observed in tissues cultured following electroporation, particularly in WT retinas, which may explain why *Venus* expression, derived from the pT2-CAGGS-*Venus* transposon, was not detectable. Significant cell death was also observed in the INL and GCL of transfected and cultured *rd10* retinas, suggesting that neurons such as bipolar cells, horizontal cells, amacrine cells, and ganglion cells die during post-electroporation cultivation, which may explain the undetectable transfection of these cell types.

When using plasmid DNA for transfection, plasmid size is inversely correlated with both transfection efficiency and cell survival.[50–53] Marie et al. reported that the miniplasmid free of antibiotic resistance markers (pFAR) enables efficient transfection and transgene expression in various cells and tissues.[54–56] In combination with the *SB* transposon system, the resulting pFAR4-ITRs vectors, which were approximately 30% smaller than the corresponding pT2 vectors, showed increased transfection efficiency for the transfer of the *Venus* transgene into HeLa cells and the *PEDF* transgene into primary retinal pigment epithelial cells.[29] We investigated the transfection efficiency of the transposon plasmids pT2-CAGGS-*Venus* (6,132 bps) and pFAR4-ITRs-CAGGS-*Venus* (4,227 bps, 31% reduced size) in *rd10* retinas and showed that the young, not yet or not fully degenerated P16 and P25 retinas could be transfected with the smaller pFAR4 transposon plasmid. In addition, transgene expression was increased 1.5-fold with the pFAR4-ITRs-CAGGS-*Venus* plasmid compared to the pT2-CAGGS-*Venus* plasmid, in agreement with the results of Pastor et al.[29] A further reduced size transposon vector, pFAR4-ITRs-SV-*Venus* (2,984 bps), was used in the expectation that transgene expression would be further increased or that the early stages of *rd10* retinas would be better transfected, which was not observed (data not shown). One reason for this may be the choice of promoter. The CAG promoter used in our plasmids, which contains elements from the cytomegalovirus (CMV) early enhancer element, chicken β-actin gene, and rabbit β-globin gene, is known for high transgene expression in mammalian cells.[57] It is considered to be efficient and versatile, whereas the CMV promoter can be associated with complex transcriptional silencing.[58,59] Previous studies showed that the CAG promoter is active in different cell types. For example, using an AAV vector, CAG promoter-driven GFP expression was observed in the inner retina of *Vldlr*$^{-/-}$ mice, a model for retinal neovascularization.[60] In our study, the pFAR4-ITRs-CAGGS-*Venus* plasmid achieved the highest transgene expression in degenerated *ex-vivo* transfected *rd10* retinas, confirming that

Figure 4. Integrity of the transfected cell membrane

(A) Electroporation of FITC-dextran 4 kDa dye was performed on *rd10* mouse retinas at developmental stages P16, P25, P61, 3M, and 6M. The flat-mounted retinas showed cells that had successfully taken up the dye, visible as green fluorescence. The magnified images show intact, clearly demarcated cells. (B) The same electroporation procedure was performed on P25, P61, 3M, and 6M WT retinas; the P16 WT stage could not be analyzed due to non-commercial availability. The flat-mounted WT retinas showed green cells that could be identified as intact, clearly distinguishable cells, indicating successful dye uptake and confirming electroporation-based transfection of WT retinas. (C) The graphs present the mean fluorescence intensity of *rd10* and WT retinas at different developmental stages. Statistical analysis reveals no significant differences between stages for both *rd10* and WT retinas ($n = 3$, one-way ANOVA test with Tukey's multiple comparisons test). Scale bars, 100 μm for whole-mount retinal images and 50 μm for the corresponding magnified images.

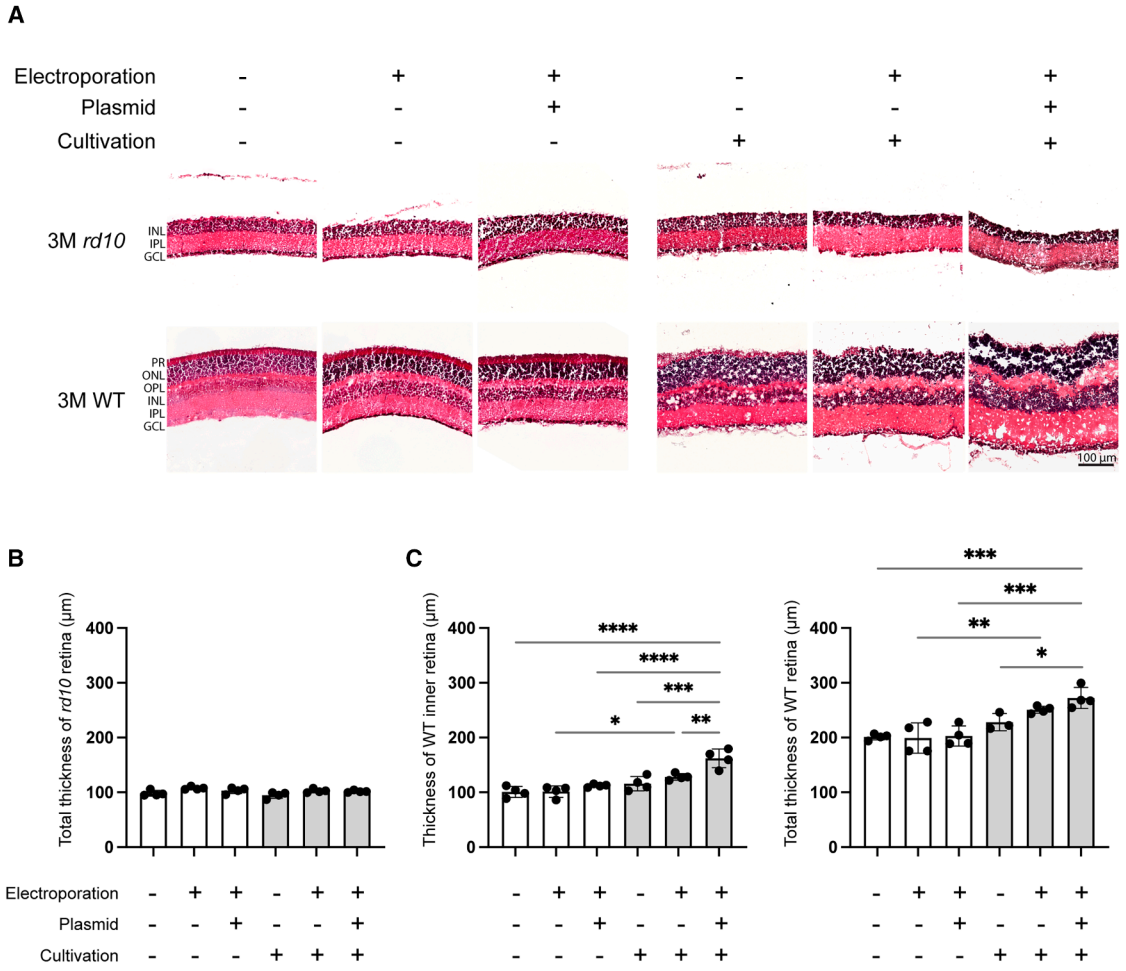

Figure 5. Morphological characteristics of transfected and cultivated 3-month-old *rd10* and WT retinas

(A) H&E staining showed the comparison of structural integrity of *rd10* and WT retinas with and without electroporation or cultivation. The degenerated *rd10* retinas showed more uniform layering after electroporation and cultivation, whereas the WT retinas showed hypertrophy and damage. (B) The graph shows the total thickness of the degenerated *rd10* retinas. There were no significant changes due to electroporation and cultivation conditions ($n = 4$, using one-way ANOVA with Tukey's multiple comparisons test). (C) The graphs show the thickness changes of inner and whole WT retinal layers with and without electroporation, with and without transposon plasmid addition, and before and after cultivation. There were no significant differences between the non-cultivated WT retinas. In the cultivation group, electroporation and plasmid addition significantly loosened the retina and increased thickness compared to cultivation alone. The thickness of electroporated (without and with transposon plasmid) and cultivated retinas increased significantly compared to the corresponding non-cultivated retinas. ($n = 4$, $^{*}p < 0.05$, $^{**}p < 0.01$, $^{***}p < 0.001$, and $^{****}p < 0.0001$, using one-way ANOVA with Tukey's multiple comparisons test). PR, photoreceptor; ONL, outer nuclear layer; OPL, outer plexiform layer; INL, inner nuclear layer; IPL, inner plexiform layer; GCL, ganglion cell layer. Scale bars, 100 µm.

both plasmid size reduction and promoter choice are critical for high transgene expression. Notably, Müller cells were still the only cell type that could be transfected despite the reduced plasmid size.

GFAP is a marker gene that is upregulated during glial activation and inflammation in retinal degeneration and is useful for analyzing retinal gliosis.[45,61–63] We showed that GFAP expression before the onset of degeneration in P16 *rd10* retinas was mainly localized to astrocytes in the GCL, in agreement with the findings of Gargini and Terzibasi.[10] After transfection of the P16 *rd10* retinas, significant structural changes were observed that were also seen in the transfected and cultivated WT retinas. As photoreceptor death progressed (P25), GFAP expression increased significantly in Müller cells, as previously reported.[46,64] In the later stages of *rd10* retinal degeneration (P61, 3M, and 6M), GFAP expression in Müller cells remained positive, consistent with previous reports of GFAP detection in Müller cells from 14-month-old *rd10* retinas.[10] However, GFAP expression was significantly lower in the older *rd10* retinas compared to P25 *rd10* retinas, similar to *Pde6b*$^{rd1/rd1}$ retinas.[65] These results suggest that transfection efficiency is related to glial activation and that the high glial activation in P25 hinders Müller cell transfection. Importantly, GFAP expression did not significantly increase after

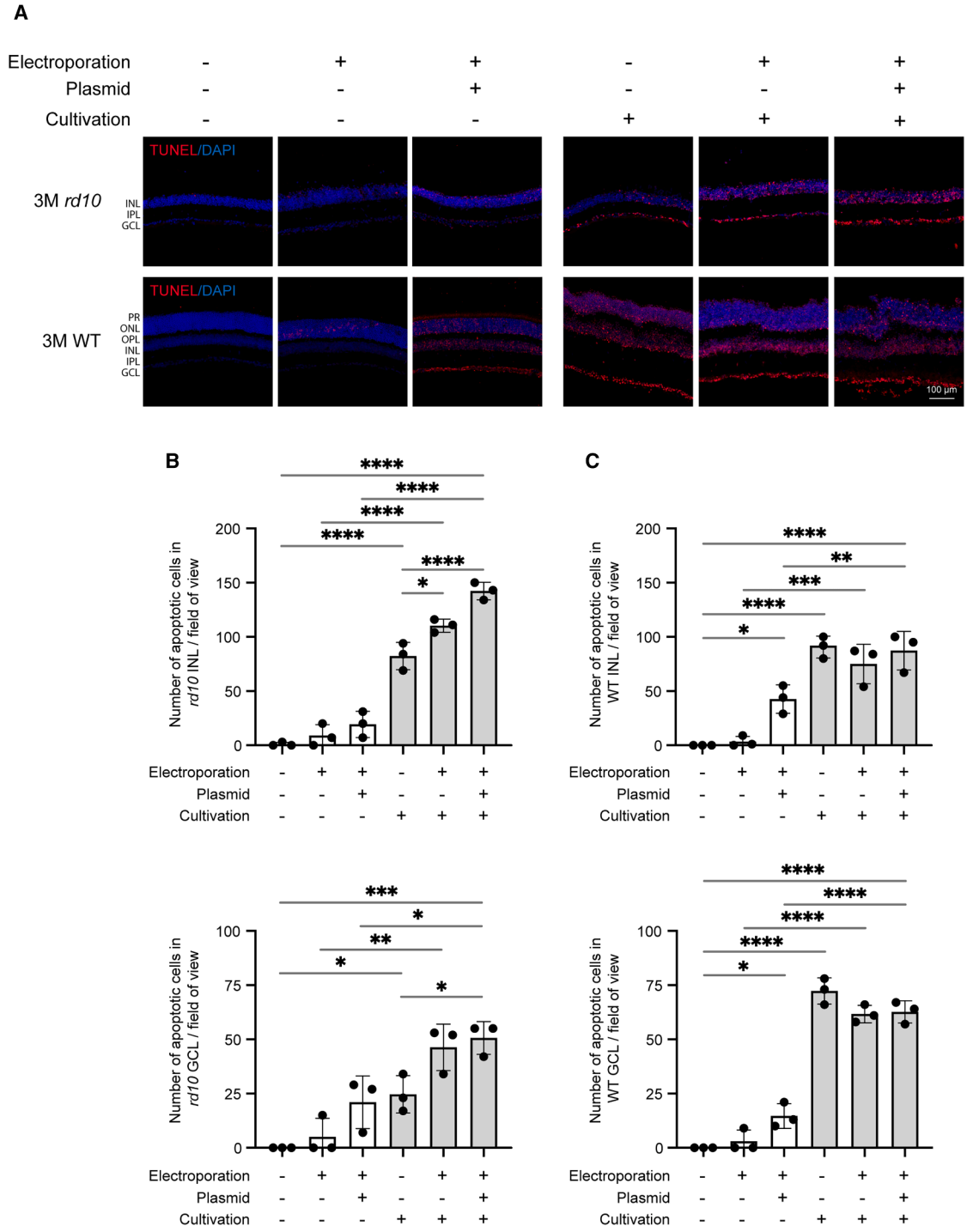

Figure 6. Cell apoptosis in transfected and cultivated 3-month-old *rd10* and WT retinas

(A) Cell apoptosis assay was performed on retinas of 3-month-old *rd10* mice and age-matched WT mice using a standardized experimental setup. The study was divided into two groups, cultivated and non-cultivated. In both groups, the effects of electroporation, transposon plasmid addition or both together were studied. In the *rd10* retinas, the total number of apoptotic cells increased in the cultivated group compared to the non-cultivated group. In the non-cultivated WT retinas, a significant increase in cell death was observed after transposon plasmid transfection compared to the two control groups. In general, an increase in apoptosis was observed after 24 h of cultivation. (B) Non-cultivated *rd10* retinas display a limited number of apoptotic cells during the transfection process. However, significant cell death was observed in both INL and GCL after

(legend continued on next page)

transfection and cultivation in late stage *rd10* retinas, indicating that our electroporation-based gene delivery method has minimal effects on retinal inflammation.

The non-viral electroporation-based gene transfer method presented here uses the *SB* transposon system to efficiently genetically modify degenerated *rd10* retinas *ex vivo*. Inherited retinal degenerations are genetically and phenotypically heterogeneous. To date, more than 250 genes with disease-causing mutations have been identified (RetNet database), which is driving the development of gene therapy treatment approaches.[66] The diversity of patient populations with different mutations and stages of retinal degeneration explains the multitude and continuous development and improvement of therapeutic approaches, which include genetic diagnostic approaches with biological therapies such as neurotrophic support, retinal cell transplantation, and optogenetics,[67–69] as well as bioengineering solutions using retinal prostheses (epiretinal Argus II retinal prostheses, subretinal implant Alpha AMS/IMS, and Bionic suprachoroidal retinal implant).[70] In contrast to mutation-specific viral gene therapy with voretigene neparvovec, the *SB* transposon-based gene transfer method used in this study pursues the idea of a more global, mutation-independent therapy combined with the advantage of stable transgene expression with improved biological safety.[18,20] To our knowledge, our study is the first to demonstrate significant differences in gene delivery efficiency during the progression of retinal degeneration in the *rd10* mouse model. The results suggest that degeneration-dependent therapeutic targets need to be considered when applying this gene therapy approach.

In the early stages of retinal degeneration, limiting retinal inflammation, which leads to low transfection efficiency, may be a critical goal.[64,71–74] In the later stages of retinal degeneration, when many or all photoreceptors are lost, neurons in the INLincluding horizontal, bipolar, and amacrine cells—survive longer and offer the possibility of improving residual vision.[75] Retinal prostheses developed for this purpose activate multiple cell types simultaneously by delivering electrical stimuli to these INL neurons, resulting in the triggering of basic visual functions. However, reactive Müller cell gliosis can form physical barriers around the electrodes, preventing electrical coupling with the retinal neurons.[76] Our study shows that glial scar formation offers the possibility of electroporation-based gene transfer into Müller cells. Retinal Müller cells, the major glial cells of the retina, play a crucial role in maintaining retinal homeostasis and supporting neuronal function. They secrete a variety of cytokines and growth factors, such as neurotrophins, basic fibroblast growth factor, PEDF, glial cell line-derived neurotrophic factor, vascular endothelial growth factor, brain-derived neurotrophic factor, and leukemia inhibitory factor, to other cell types in the retina that protect degenerating neurons.[77–79] In addition, Müller cells interact with all classes of retinal neurons and persist into the late stages of retinal degeneration, making them ideal candidates for Müller cell-specific gene therapy.[78] We therefore see the potential to combine Müller cell-specific gene therapy with retinal prostheses. This involves the use of implantable electrodes for stimulation and electroporation, which could improve therapeutic outcomes in the late stages of degenerative retinal diseases.

However, there are some limitations to consider. The long-term health of the retina after transfection was not investigated in this study. Retinal cells are subjected to homeostatic stress and apoptosis during cultivation, which limits the study of effects on Müller cell physiology and overall retinal function during electroporation-based gene transfer. Although electroporation is a powerful tool in animal models, its application in human clinical practice is limited due to the invasive nature of the procedure required to place electrodes close enough to target retinal cells effectively.[80] Our subsequent studies will focus on *ex-vivo* and *in-vivo* investigations, the transfer of therapeutic genes into the degenerated *rd10* retina and their effects on retinal structure and function, and the use of retinal prosthesis analogue electrode array structures for retinal electroporation.

MATERIALS AND METHODS

Animals

In this study, B6.CXB1-Pde6b*rd10*/J (*rd10*) mice and C57BL/6J WT mice were used. Male and female *rd10* mice were bred at the Institute of Laboratory Animal Science (Faculty of Medicine, RWTH Aachen University, Aachen, Germany); male and female WT mice were obtained from Janvier Labs (Le Genest-Saint-Isle, France). All experiments were performed in accordance with the ARVO Statement for the Use of Animals in Ophthalmic and Vision Research after approval (40135A4) of the Ethics Committee of the Institute of Laboratory Animal Science (Faculty of Medicine, RWTH Aachen University). Animals were housed under controlled light conditions (12:12 h light/dark cycle) at a room temperature (RT) of 21°C–23°C and a humidity of 35%–65%. Water and food were provided *ad libitum*, and cages were cleaned once a week.

To investigate the effects of electroporation on the different stages of retinal degeneration, *rd10* and age-matched WT retinas were analyzed at P16, P25, P61, 3M, and 6M. A total of 194 mice (388 retinas) were used in this study. For the final statistical analysis, 325 retinas were included, divided into 201 retinas for plasmid electroporation; 27 retinas for FITC-dextran electroporation; and 97 retinas for histology, immunofluorescence, and TUNEL staining. It is important to note that some retinas used for plasmid electroporation

cultivation ($n = 3$, $^{*}p < 0.05$, $^{**}p < 0.01$, $^{***}p < 0.001$, and $^{****}p < 0.0001$, using one-way ANOVA with Tukey's multiple comparisons test). (C) In non-cultivated WT retinas, a significant increase in the number of apoptotic cells was observed in both INL and GCL after transposon plasmid transfection. After 24 h of cultivation, a significant increase in apoptosis was observed throughout the retina, regardless of electroporation without or with transposon plasmid addition ($n = 3$, $^{*}p < 0.05$, $^{**}p < 0.01$, $^{***}p < 0.001$, and $^{****}p < 0.0001$, using one-way ANOVA with Tukey's multiple comparisons test). PR, photoreceptor; ONL, outer nuclear layer; OPL, outer plexiform layer; INL, inner nuclear layer; IPL, inner plexiform layer; GCL, ganglion cell layer. Scale bars, 100 μm.

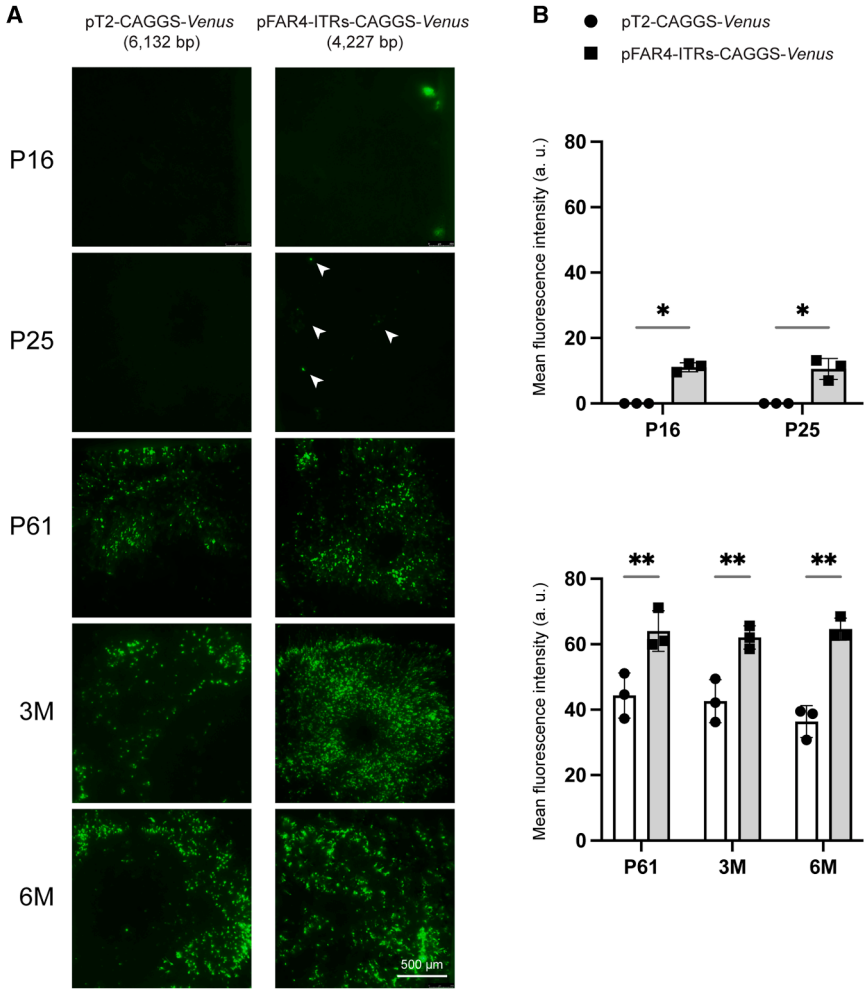

Figure 7. Effect of transposon plasmid size on transfection efficiency in *rd10* retinas of different ages

(A) The transposon plasmids pT2-CAGGS-*Venus* (6,132 bps) and pFAR4-ITRs-CAGGS-*Venus* (4,227 bps) were used to evaluate the effect of plasmid size on electroporation efficiency. The fluorescent cells in flat-mounted retinas indicate successful transfection, which occurred with pT2-CAGGS-*Venus* exclusively in older *rd10* mice (from P61), whereas no transfected cells were detectable in the earlier stages P16 and P25. White arrowheads indicate the expression of pFAR4-ITRs-CAGGS-*Venus* observed in P25 stages of *rd10* mice. (B) Quantitative analysis of the transfection efficiency in young and adult *rd10* retinas was conducted by measuring the mean fluorescence intensity. The transfection efficiency of the pFAR4-ITRs-CAGGS-*Venus* transposon plasmid was significantly higher compared to the pT2-CAGGS-*Venus* plasmid ($n = 3$, $^{*}p < 0.05$, and $^{**}p < 0.01$, using two-way ANOVA with uncorrected Fisher's least significant difference for young *rd10* retinas and two-way ANOVA with Tukey's multiple comparisons test for adult *rd10* retinas). Scale bars, 500 µm.

were also sectioned for subsequent immunofluorescence staining, but these were not included again in the quantification of animal numbers. Each experiment included both male and female mice. The difference of 63 retinas was used to establish and optimize the experimental protocols.

SB transposon-based plasmids

The *SB* transposon system used in this study consists of the *SB100X* transposase plasmid (4,752 bp)[81] and two transposon plasmids, both encoding the yellow fluorescent protein (YFP, *Venus*) driven by the CAGGS promoter: pT2-CAGGS-*Venus* (6,132 bp)[81] and pFAR4-ITRs-CAGGS-*Venus* (4,227 bp), a derivative of the antibiotic-free pFAR4 vector[54] containing the ITRs extracted from pT2/HB.[29] A total plasmid concentration of 0.1 µg/µL was used per electroporation, with a ratio of 1:16 between the *SB100X* transposase plasmid and the *Venus* transposon plasmid.[28] Plasmid DNA was purified using plasmid purification kits (QIAGEN, Hilden, Germany) suitable for applications such as transfection, according to the manufacturer's protocol.

Electroporation system

The NEPA21 type II electroporator (Nepa Gene, Ichikawa, Japan) and tissue-specific electrodes were used for *ex-vivo* retinal electroporation. A lower Petri dish Round Platinum Plate Electrode with Embankment Well (7 mm diameter; Nepa Gene) and an upper Cover Round Platinum Plate Electrode (5 mm diameter; Nepa Gene) were used. During electroporation, the upper electrode was precisely lowered to the same height using a scaled micromanipulator (World Precision Instruments, Sarasota, FL, United States).

E-vivo retinal electroporation and cultivation

Sterile PBS (PAN Biotech, Aidenbach, Germany) and Opti-MEM Reduced-Serum Medium (Gibco, Life Technologies, MA, United States) were used as buffers for electroporation. Sterile Ames' medium (Sigma-Aldrich, St. Louis, MO, United States) was prepared according to the manufacturer's recommendations for isolation and tissue culture of mouse retina (Ames and Nesbett 1981). The culture solution contained 1% N2 (Gibco, Life Technologies) and 2% B27 (Gibco, Life Technologies) diluted in Ames' medium.

Mice were deeply anesthetized and sacrificed with an overdose of isoflurane (AbbVie, Wiesbaden, Germany). Enucleated eyes were incised circularly along the limbus. The retina was carefully separated from the eyecup and placed on a 3 × 3 mm^2 nitrocellulose frame (GE Healthcare Europe, Freiburg, Germany) to allow for a better transition and to optimize preservation of the retinal

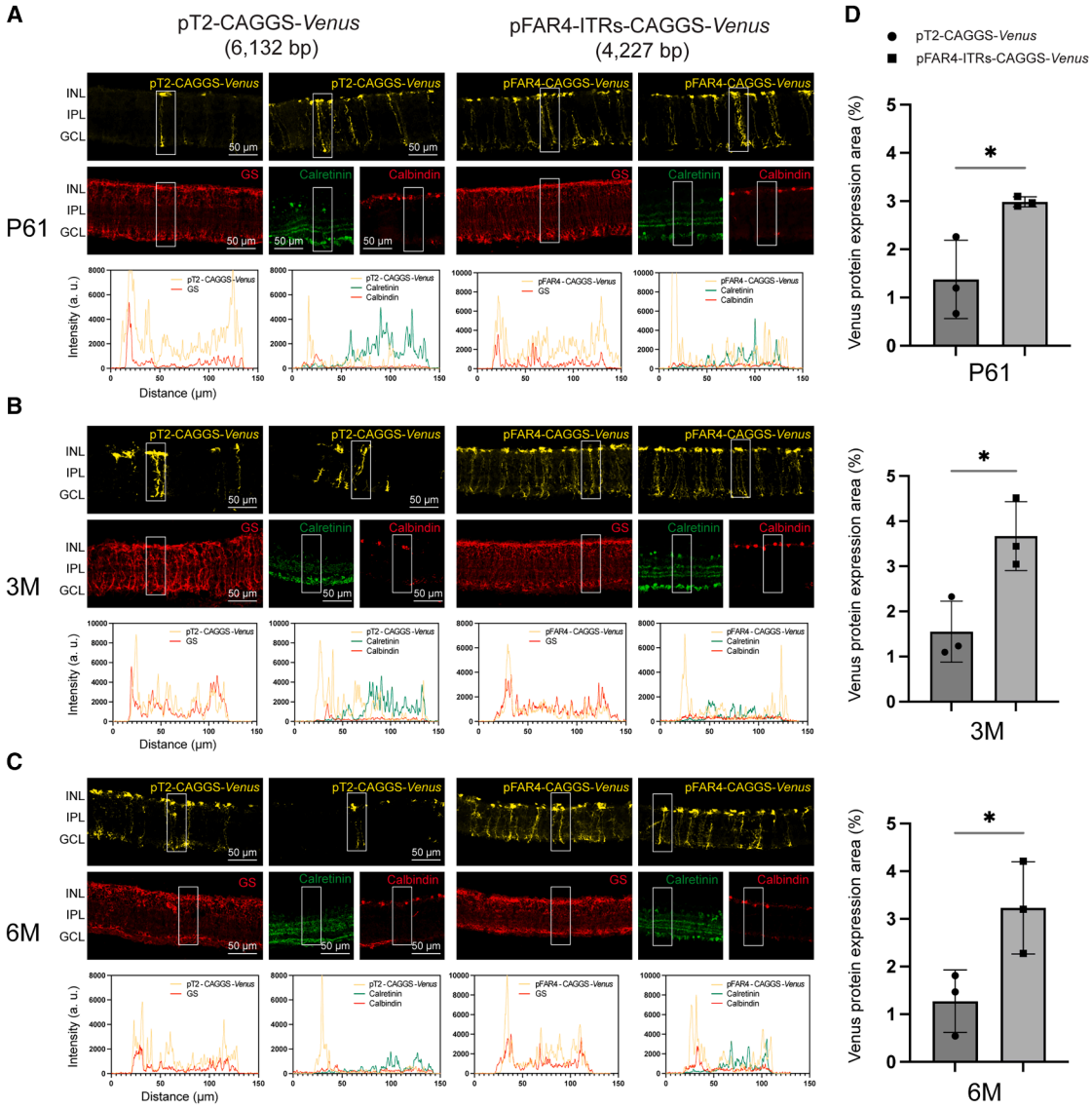

Figure 8. Effect of plasmid size on the transfected cell type in adult *rd10* retinas

(A–C) The different-sized plasmids pT2-CAGGS-*Venus* and pFAR4-ITRs-CAGGS-*Venus* were introduced into (A) P61, (B) 3M, and (C) 6M old *rd10* retinas by electroporation. Transfected cells were identified with anti-GS (Müller cells), anti-calretinin (amacrine cells), and anti-calbindin (horizontal cells) antibodies after 24 h of cultivation, followed by co-localization analysis. Yellow fluorescent protein transfected cells were distributed throughout the retinal layers at all ages and for all plasmids used. They were analyzed in the whole retinal section and the transfected cells indicated by the white frames were subjected to co-localization analysis with the three retinal cell markers mentioned. These analyses showed that the transfected cells were co-labeled only with anti-GS. Overall, a high concordance of Müller cells with the transfected cells was found, independent of plasmid size. (D) The corresponding quantitative analysis was performed by measuring Venus protein expression area. The graphs show that retinas transfected with the pFAR4-ITRs-CAGGS-*Venus* plasmid had a higher number of transfected Müller cells compared to those transfected with the pT2-CAGGS-*Venus* plasmid ($n = 3$, $^*p < 0.05$, using unpaired two-tailed t test). INL, inner nuclear layer; IPL, inner plexiform layer; GCL, ganglion cell layer. Scale bars, 50 µm.

morphology. The mounted retina was then carefully placed photoreceptor side down on a culture insert (Corning, ME, United States), which was then placed on the lower plate electrode.

The reservoir of the lower plate electrode was filled with 40 µL of the plasmid mixture containing the *SB100X* transposase plasmid and the *Venus* transposon plasmid diluted in PBS or Opti-MEM buffer. A further 10 µL of the plasmid mixture was added to the mounted retinal tissue. The micromanipulator-controlled upper plate electrode was then carefully lowered onto the 10 µL drop of plasmid mixture. The distance between the electrodes is 1.2 mm. The electric impedance between the retinal tissue and the electroporation buffer

was measured with values between 95 and 115 Ω. The following electroporation parameters were used: 5–15 V (voltage), 5 ms (length), 50 ms (interval), 1–2 (number), 10% (decay rate), +/− (polarity) for the poring pulse; 5–15 V, 50 ms, 50 ms, 1–5, 40%, +/− for the transfer pulse. The parameters recorded included the output voltages, currents, and energy of the pulses after electroporation. The electroporated retina was incubated for 24 h on the culture insert in a 6-well cell culture plate with 1 mL culture medium/well at 37°C in a humidified atmosphere of 95% air and 5% CO_2. Transfection efficiency of the flat-mount retinas was assessed one day after incubation using a fluorescence microscope (Leica DMi8; Leica, Wetzlar, Germany).

FITC-dextran electroporation

To investigate electroporation in *rd10* and WT mice, flat-mounted retinas were electroporated with fluorescein isothiocyanate (FITC)-dextran (FITC-dextran). Dextran, a glucose polymer of varying molecular weights, is widely used to assess pore size and membrane permeability and integrity due to its low toxicity and immunogenicity.[82] Dextran is usually conjugated with fluorophores such as FITC and allows detection by fluorescence microscopy.[83–85] In our study, FITC-dextran with a molecular weight of 4 kDa (FD4; Merck, Darmstadt, Germany) was dissolved in sterile PBS and prepared at a concentration of 10 mg/mL. The final concentration used for electroporation was 4 mg/mL, diluted in Opti-MEM electroporation buffer. The electroporation parameters were applied in the same way as described previously. After electroporation, flat-mounted retinas were rinsed twice in Ames' medium to remove non-incorporated FITC-dextran before direct examination by confocal fluorescence microscopy. A negative control treated with FITC-dextran but not electroporated was included in each experiment.

Histology and immunofluorescence staining

Retinal tissue was fixed in 4% paraformaldehyde (PFA) for 30 min at RT and then rinsed twice in PBS. Subsequently, the retina was cryoprotected in PBS solutions containing 10%, 20%, and 30% sucrose for 15, 15, and 30 min, respectively. The retinal tissue was then embedded in pure Tissue-Tek OCT (Sakura, Japan) and stored at −20°C. Vertical sections of retina cryoblocks were cut at 10 μm for histology and 20 μm for immunofluorescence staining using a cryostat and mounted on Superfrost Plus slides (Fisher Scientific, Germany).

Histological assessment was performed using H&E staining to evaluate retinal morphology after electroporation and cultivation. Sections were stained with hematoxylin for 10 min and eosin for 8 min, and then washed with tap water for 10 min and coverslipped (VWR International, Radnor, PA, United States). Images were captured using a Slide Scanner (PreciPoint, Garching, Germany).

For immunofluorescence analysis, tissue sections were incubated overnight at RT with primary antibodies diluted in incubation solution BTA (5% bovine serum albumin [BSA; Carl Roth, Karlsruhe, Germany], 0.5% Triton X-100 [Merck], and 0.05% NaN_3 [Merck] in PBS). Sections were washed with PBS and incubated with secondary antibodies diluted in BTA for 1 h at RT, washed in PBS, and coverslipped with Aqua Polymount (Polysciences, Warrington, PA, United States). Sections were analyzed and photographed using a confocal fluorescence microscope (Zeiss LSM 980 Airyscan 2; Zeiss, Oberkochen, Germany). Primary antibodies included anti-GS (anti-glutamine synthetase, mouse IgG2a, 1:500; BD Biosciences, Franklin Lakes, NJ, United States), anti-GFAP (anti-glial fibrillary acidic protein, chicken polyclonal, 1: 500; Novus Biologicals, Centennial, Co., United States), anti-CabP (anti-calbindin, mouse monoclonal, 1:500; Merck), and anti-Cal (anti-calretinin, rabbit polyclonal, 1:500; Abcam, Cambridge, United Kingdom). The YFP *Venus* did not require antibody labeling. Secondary antibodies included donkey anti-mouse Cy3 (1: 200; BIOZOL, Eching, Germany), goat anti-chicken 647 (1:200; BIOZOL), and donkey anti-rabbit 647 (1: 200; BIOZOL). Cell nuclei were counterstained with 1 μg/mL 4′,6-diamidino-2-phenylindole (DAPI; Merck).

TUNEL apoptosis assay

Cell apoptosis in transfected retinas was determined using the *In Situ* Cell Death Detection Kit, TMR red (Merck). Briefly, retinal sections were incubated in permeabilization solution (0.1% Triton X-100) at RT for 5 min and rinsed twice with PBS. Subsequently, 100 μL of TUNEL reaction mixture (10 μL enzyme solution plus 90 μL label solution) was added to each slide and incubated overnight at RT in the dark. Negative controls were treated with 100 μL of label solution only. Positive controls were incubated with recombinant DNase I (RNase-Free DNase Set; QIAGEN) for 5 min after permeabilization, then rinsed and mixed with the reaction mixture. The next day, slides were washed three times in PBS and incubated with 1 μg/mL DAPI for one hour. Fluorescence signals were captured using a confocal fluorescence microscope (Zeiss LSM 980 Airyscan 2; Zeiss). The number of apoptotic cells was quantified per field of view (25×10^4 μm^2).

Data analysis and statistics

Statistical analyses were conducted using GraphPad Prism software 10 (GraphPad, La Jolla, CA, United States). Results are described as mean ± standard deviation (SD). The corresponding statistical tests are indicated in the figure legends. A p value <0.05 was considered statistically significant.

DATA AND CODE AVAILABILITY

All data essential for the reproducibility of this study are included within this manuscript. Additional information can be provided upon request by contacting the corresponding author.

ACKNOWLEDGMENTS

This work was supported by the Confocal Microscope Facility and the Immunohistochemistry Facility, core facilities of the Interdisciplinary Center for Clinical Research (IZKF) Aachen within the Faculty of Medicine at RWTH Aachen University. The authors thank Anne Freialdenhoven, Antje Schiefer, and Alicia Hühnlein (Department of Ophthalmology, University Hospital RWTH Aachen) for excellent technical assistance. This work was funded by the China Scholarship Council (no. 202208080251) and is part of a graduate school funded by the Deutsche Forschungsgemeinschaft DFG under GRK 2610/01. The results shown here are part of the doctoral thesis of J.Z.

AUTHOR CONTRIBUTIONS

Conceptualization, P.W. and S.J.; data curation, J.Z. and S.J.; formal analysis, J.Z.; funding acquisition, F.M., P.W., and S.J.; investigation, J.Z.; methodology, J.Z., F.M., and S.J.; project administration, S.J.; resources, C.M., Z.I., and G.T.; supervision, P.W. and S.J.; validation, J.Z., F.M., P.W., and S.J.; visualization, J.Z.; writing – original draft, J.Z.; writing – review & editing, all authors.

DECLARATION OF INTERESTS

Z.I. is a co-inventor on several *SB*-related patents.

SUPPLEMENTAL INFORMATION

Supplemental information can be found online at https://doi.org/10.1016/j.omtn.2025.102616.

REFERENCES

1. Hartong, D.T., Berson, E.L., and Dryja, T.P. (2006). Retinitis pigmentosa. Lancet *368*, 1795–1809. https://doi.org/10.1016/s0140-6736(06)69740-7.
2. Bunker, C.H., Berson, E.L., Bromley, W.C., Hayes, R.P., and Roderick, T.H. (1984). Prevalence of retinitis pigmentosa in Maine. Am. J. Ophthalmol. *97*, 357–365. https://doi.org/10.1016/0002-9394(84)90636-6.
3. Horsager, A., Greenwald, S.H., Weiland, J.D., Humayun, M.S., Greenberg, R.J., McMahon, M.J., Boynton, G.M., and Fine, I. (2009). Predicting visual sensitivity in retinal prosthesis patients. Investig. Ophthalmol. Vis. Sci. *50*, 1483–1491. https://doi.org/10.1167/iovs.08-2595.
4. Wang, A.L., Knight, D.K., Vu, T.T.T., and Mehta, M.C. (2019). Retinitis Pigmentosa: Review of Current Treatment. Int. Ophthalmol. Clin. *59*, 263–280. https://doi.org/10.1097/IIO.0000000000000256.
5. Dias, M.F., Joo, K., Kemp, J.A., Fialho, S.L., da Silva Cunha, A., Jr., Woo, S.J., and Kwon, Y.J. (2018). Molecular genetics and emerging therapies for retinitis pigmentosa: Basic research and clinical perspectives. Prog. Retin. Eye Res. *63*, 107–131. https://doi.org/10.1016/j.preteyeres.2017.10.004.
6. Derkach, A.V., and Trofimova, S.V. (2019). [Modern approaches to the retinitis pigmentosa treatment in the older age patients (literature review). Adv. Gerontol. *32*, 1017–1022.
7. Chang, B., Hawes, N.L., Pardue, M.T., German, A.M., Hurd, R.E., Davisson, M.T., Nusinowitz, S., Rengarajan, K., Boyd, A.P., Sidney, S.S., et al. (2007). Two mouse retinal degenerations caused by missense mutations in the beta-subunit of rod cGMP phosphodiesterase gene. Vision Res. *47*, 624–633. https://doi.org/10.1016/j.visres.2006.11.020.
8. Chang, B., Hawes, N.L., Hurd, R.E., Davisson, M.T., Nusinowitz, S., and Heckenlively, J.R. (2002). Retinal degeneration mutants in the mouse. Vision Res. *42*, 517–525. https://doi.org/10.1016/s0042-6989(01)00146-8.
9. Wang, T., Reingruber, J., Woodruff, M.L., Majumder, A., Camarena, A., Artemyev, N.O., Fain, G.L., and Chen, J. (2018). The PDE6 mutation in the rd10 retinal degeneration mouse model causes protein mislocalization and instability and promotes cell death through increased ion influx. J. Biol. Chem. *293*, 15332–15346. https://doi.org/10.1074/jbc.RA118.004459.
10. Gargini, C., Terzibasi, E., Mazzoni, F., and Strettoi, E. (2007). Retinal organization in the retinal degeneration 10 (rd10) mutant mouse: a morphological and ERG study. J. Comp. Neurol. *500*, 222–238. https://doi.org/10.1002/cne.21144.
11. Verma, I.M., and Somia, N. (1997). Gene therapy – promises, problems and prospects. Nature *389*, 239–242. https://doi.org/10.1038/38410.
12. Campbell, J.P., McFarland, T.J., and Stout, J.T. (2016). Ocular Gene Therapy. Dev. Ophthalmol. *55*, 317–321. https://doi.org/10.1159/000434698.
13. Martinez Velazquez, L.A., and Ballios, B.G. (2021). The Next Generation of Molecular and Cellular Therapeutics for Inherited Retinal Disease. Int. J. Mol. Sci. *22*, 11542. https://doi.org/10.3390/ijms222111542.
14. Mendell, J.R., Al-Zaidy, S.A., Rodino-Klapac, L.R., Goodspeed, K., Gray, S.J., Kay, C.N., Boye, S.L., Boye, S.E., George, L.A., Salabarria, S., et al. (2021). Current Clinical Applications of In Vivo Gene Therapy with AAVs. Mol. Ther. *29*, 464–488. https://doi.org/10.1016/j.ymthe.2020.12.007.
15. Schneider, N., Sundaresan, Y., Gopalakrishnan, P., Beryozkin, A., Hanany, M., Levanon, E.Y., Banin, E., Ben-Aroya, S., and Sharon, D. (2022). Inherited retinal diseases: Linking genes, disease-causing variants, and relevant therapeutic modalities. Prog. Retin. Eye Res. *89*, 101029. https://doi.org/10.1016/j.preteyeres.2021.101029.
16. Sobh, M., Lagali, P.S., Ghiasi, M., Montroy, J., Dollin, M., Hurley, B., Leonard, B.C., Dimopoulos, I., Lafreniere, M., Fergusson, D.A., et al. (2023). Safety and Efficacy of Adeno-Associated Viral Gene Therapy in Patients With Retinal Degeneration: A Systematic Review and Meta-Analysis. Transl. Vis. Sci. Technol. *12*, 24. https://doi.org/10.1167/tvst.12.11.24.
17. Wang, D., Tai, P.W.L., and Gao, G. (2019). Adeno-associated virus vector as a platform for gene therapy delivery. Nat. Rev. Drug Discov. *18*, 358–378. https://doi.org/10.1038/s41573-019-0012-9.
18. Amberger, M., and Ivics, Z. (2020). Latest Advances for the Sleeping Beauty Transposon System: 23 Years of Insomnia but Prettier than Ever: Refinement and Recent Innovations of the Sleeping Beauty Transposon System Enabling Novel, Nonviral Genetic Engineering Applications. Bioessays *42*, e2000136. https://doi.org/10.1002/bies.202000136.
19. Izsvák, Z., and Ivics, Z. (2004). Sleeping beauty transposition: biology and applications for molecular therapy. Mol. Ther. *9*, 147–156. https://doi.org/10.1016/j.ymthe.2003.11.009.
20. Izsvak, Z., Hackett, P.B., Cooper, L.J., and Ivics, Z. (2010). Translating Sleeping Beauty transposition into cellular therapies: victories and challenges. Bioessays *32*, 756–767. https://doi.org/10.1002/bies.201000027.
21. Ivics, Z., Hackett, P.B., Plasterk, R.H., and Izsvák, Z. (1997). Molecular reconstruction of Sleeping Beauty, a Tc1-like transposon from fish, and its transposition in human cells. Cell *91*, 501–510. https://doi.org/10.1016/s0092-8674(00)80436-5.
22. Ivics, Z., and Izsvák, Z. (2015). Sleeping Beauty Transposition. Microbiol. Spectr. *3*, MDNA3-0042-2014. https://doi.org/10.1128/microbiolspec.MDNA3-0042-2014.
23. Vigdal, T.J., Kaufman, C.D., Izsvák, Z., Voytas, D.F., and Ivics, Z. (2002). Common physical properties of DNA affecting target site selection of sleeping beauty and other Tc1/mariner transposable elements. J. Mol. Biol. *323*, 441–452. https://doi.org/10.1016/s0022-2836(02)00991-9.
24. Yant, S.R., Wu, X., Huang, Y., Garrison, B., Burgess, S.M., and Kay, M.A. (2005). High-resolution genome-wide mapping of transposon integration in mammals. Mol. Cell Biol. *25*, 2085–2094. https://doi.org/10.1128/mcb.25.6.2085-2094.2005.
25. Gogol-Döring, A., Ammar, I., Gupta, S., Bunse, M., Miskey, C., Chen, W., Uckert, W., Schulz, T.F., Izsvák, Z., and Ivics, Z. (2016). Genome-wide Profiling Reveals Remarkable Parallels Between Insertion Site Selection Properties of the MLV Retrovirus and the piggyBac Transposon in Primary Human CD4(+) T Cells. Mol. Ther. *24*, 592–606. https://doi.org/10.1038/mt.2016.11.
26. Thumann, G., Stöcker, M., Maltusch, C., Salz, A.K., Barth, S., Walter, P., and Johnen, S. (2010). High efficiency non-viral transfection of retinal and iris pigment epithelial cells with pigment epithelium-derived factor. Gene Ther. *17*, 181–189. https://doi.org/10.1038/gt.2009.124.
27. Thumann, G., Harmening, N., Prat-Souteyrand, C., Marie, C., Pastor, M., Sebe, A., Miskey, C., Hurst, L.D., Diarra, S., Kropp, M., et al. (2017). Engineering of PEDF-Expressing Primary Pigment Epithelial Cells by the SB Transposon System Delivered by pFAR4 Plasmids. Mol. Ther. Nucleic Acids *6*, 302–314. https://doi.org/10.1016/j.omtn.2017.02.002.
28. Johnen, S., Izsvák, Z., Stöcker, M., Harmening, N., Salz, A.K., Walter, P., and Thumann, G. (2012). Sleeping Beauty transposon-mediated transfection of retinal and iris pigment epithelial cells. Investig. Ophthalmol. Vis. Sci. *53*, 4787–4796. https://doi.org/10.1167/iovs.12-9951.
29. Pastor, M., Johnen, S., Harmening, N., Quiviger, M., Pailloux, J., Kropp, M., Walter, P., Ivics, Z., Izsvák, Z., Thumann, G., et al. (2018). The Antibiotic-free pFAR4 Vector Paired with the Sleeping Beauty Transposon System Mediates Efficient Transgene Delivery in Human Cells. Mol. Ther. Nucleic Acids *11*, 57–67. https://doi.org/10.1016/j.omtn.2017.12.017.
30. Kropp, M., Harmening, N., Bascuas, T., Johnen, S., De Clerck, E., Fernández, V., Ronchetti, M., Cadossi, R., Zanini, C., Scherman, D., et al. (2022). GMP-Grade Manufacturing and Quality Control of a Non-Virally Engineered Advanced Therapy Medicinal Product for Personalized Treatment of Age-Related Macular

Degeneration. Biomedicines *10*, 2777. https://doi.org/10.3390/biomedicines10112777.

31. Du, X., Butler, A.G., and Chen, H.Y. (2024). Cell-cell interaction in the pathogenesis of inherited retinal diseases. Front. Cell Dev. Biol. *12*, 1332944. https://doi.org/10.3389/fcell.2024.1332944.

32. Löffler, K., Schäfer, P., Völkner, M., Holdt, T., and Karl, M.O. (2015). Age-dependent Müller glia neurogenic competence in the mouse retina. Glia *63*, 1809–1824. https://doi.org/10.1002/glia.22846.

33. Elmasry, K., Moustafa, M., and Al-Shabrawey, M. (2022). Retinal Explant of the Adult Mouse Retina as an Ex Vivo Model for Studying Retinal Neurovascular Diseases. J. Vis. Exp. https://doi.org/10.3791/63966.

34. Schaeffer, J., Delpech, C., Albert, F., Belin, S., and Nawabi, H. (2020). Adult Mouse Retina Explants: From ex vivo to in vivo Model of Central Nervous System Injuries. Front. Mol. Neurosci. *13*, 599948. https://doi.org/10.3389/fnmol.2020.599948.

35. Urbanskas, E., Jakštys, B., Venckus, J., Malakauskaitė, P., Šatkauskienė, I., Morkvėnaitė-Vilkončienė, I., and Šatkauskas, S. (2024). Interplay between Electric Field Strength and Number of Short-Duration Pulses for Efficient Gene Electrotransfer. Pharmaceuticals *17*, 825. https://doi.org/10.3390/ph17070825.

36. Pavlin, M., and Kandušer, M. (2015). New insights into the mechanisms of gene electrotransfer–experimental and theoretical analysis. Sci. Rep. *5*, 9132. https://doi.org/10.1038/srep09132.

37. Jordan, E.T., Collins, M., Terefe, J., Ugozzoli, L., and Rubio, T. (2008). Optimizing electroporation conditions in primary and other difficult-to-transfect cells. J. Biomol. Tech. *19*, 328–334.

38. Jin, K., and Xiang, M. (2012). In vitro explant culture and related protocols for the study of mouse retinal development. Methods Mol. Biol. *884*, 155–165. https://doi.org/10.1007/978-1-61779-848-1_10.

39. Stone, M.L., Lee, H.H., and Levine, E. (2024). An agarose disk electroporation method for ex vivo retinal tissue cultured at the air-liquid interface reveals electrical stimulus-induced cell cycle reentry in retinal cells. Preprint at: bioRxiv. https://doi.org/10.1101/2023.12.21.572865

40. Hyder, I., Eghbalsaied, S., and Kues, W.A. (2020). Systematic optimization of square-wave electroporation conditions for bovine primary fibroblasts. BMC Mol. Cell Biol. *21*, 9. https://doi.org/10.1186/s12860-020-00254-5.

41. Eghbalsaied, S., Hyder, I., and Kues, W.A. (2020). A versatile bulk electrotransfection protocol for murine embryonic fibroblasts and iPS cells. Sci. Rep. *10*, 13332. https://doi.org/10.1038/s41598-020-70258-w.

42. Matsuda, T., and Cepko, C.L. (2004). Electroporation and RNA interference in the rodent retina in vivo and in vitro. Proc. Natl. Acad. Sci. USA *101*, 16–22. https://doi.org/10.1073/pnas.2235688100.

43. Tworig, J.M., and Feller, M.B. (2021). Müller Glia in Retinal Development: From Specification to Circuit Integration. Front. Neural Circuits *15*, 815923. https://doi.org/10.3389/fncir.2021.815923.

44. MacDonald, R.B., Charlton-Perkins, M., and Harris, W.A. (2017). Mechanisms of Müller glial cell morphogenesis. Curr. Opin. Neurobiol. *47*, 31–37. https://doi.org/10.1016/j.conb.2017.08.005.

45. Bringmann, A., Pannicke, T., Grosche, J., Francke, M., Wiedemann, P., Skatchkov, S. N., Osborne, N.N., and Reichenbach, A. (2006). Müller cells in the healthy and diseased retina. Prog. Retin. Eye Res. *25*, 397–424. https://doi.org/10.1016/j.preteyeres.2006.05.003.

46. Phillips, M.J., Otteson, D.C., and Sherry, D.M. (2010). Progression of neuronal and synaptic remodeling in the rd10 mouse model of retinitis pigmentosa. J. Comp. Neurol. *518*, 2071–2089. https://doi.org/10.1002/cne.22322.

47. Dezawa, M., Takano, M., Negishi, H., Mo, X., Oshitari, T., and Sawada, H. (2002). Gene transfer into retinal ganglion cells by in vivo electroporation: a new approach. Micron *33*, 1–6. https://doi.org/10.1016/s0968-4328(01)00002-6.

48. Batista Napotnik, T., and Miklavčič, D. (2018). In vitro electroporation detection methods - An overview. Bioelectrochemistry *120*, 166–182. https://doi.org/10.1016/j.bioelechem.2017.12.005.

49. Graziadei, L., Burfeind, P., and Bar-Sagi, D. (1991). Introduction of unlabeled proteins into living cells by electroporation and isolation of viable protein-loaded cells using dextran-fluorescein isothiocyanate as a marker for protein uptake. Anal. Biochem. *194*, 198–203. https://doi.org/10.1016/0003-2697(91)90168-s.

50. Lesueur, L.L., Mir, L.M., and André, F.M. (2016). Overcoming the Specific Toxicity of Large Plasmids Electrotransfer in Primary Cells In Vitro. Mol. Ther. Nucleic Acids *5*, e291. https://doi.org/10.1038/mtna.2016.4.

51. Kreiss, P., Cameron, B., Rangara, R., Mailhe, P., Aguerre-Charriol, O., Airiau, M., Scherman, D., Crouzet, J., and Pitard, B. (1999). Plasmid DNA size does not affect the physicochemical properties of lipoplexes but modulates gene transfer efficiency. Nucleic Acids Res. *27*, 3792–3798. https://doi.org/10.1093/nar/27.19.3792.

52. Chabot, S., Orio, J., Schmeer, M., Schleef, M., Golzio, M., and Teissié, J. (2013). Minicircle DNA electrotransfer for efficient tissue-targeted gene delivery. Gene Ther. *20*, 62–68. https://doi.org/10.1038/gt.2011.215.

53. Hornstein, B.D., Roman, D., Arévalo-Soliz, L.M., Engevik, M.A., and Zechiedrich, L. (2016). Effects of Circular DNA Length on Transfection Efficiency by Electroporation into HeLa Cells. PLoS One *11*, e0167537. https://doi.org/10.1371/journal.pone.0167537.

54. Marie, C., Vandermeulen, G., Quiviger, M., Richard, M., Préat, V., and Scherman, D. (2010). pFARs, plasmids free of antibiotic resistance markers, display high-level transgene expression in muscle, skin and tumour cells. J. Gene Med. *12*, 323–332. https://doi.org/10.1002/jgm.1441.

55. Quiviger, M., Arfi, A., Mansard, D., Delacotte, L., Pastor, M., Scherman, D., and Marie, C. (2014). High and prolonged sulfamidase secretion by the liver of MPS-IIIA mice following hydrodynamic tail vein delivery of antibiotic-free pFAR4 plasmid vector. Gene Ther. *21*, 1001–1007. https://doi.org/10.1038/gt.2014.75.

56. Marie, C., and Scherman, D. (2024). Antibiotic-Free Gene Vectors: A 25-Year Journey to Clinical Trials. Genes *15*, 261. https://doi.org/10.3390/genes15030261.

57. Foecking, M.K., and Hofstetter, H. (1986). Powerful and versatile enhancer-promoter unit for mammalian expression vectors. Gene *45*, 101–105. https://doi.org/10.1016/0378-1119(86)90137-x.

58. Niwa, H., Yamamura, K., and Miyazaki, J. (1991). Efficient selection for high-expression transfectants with a novel eukaryotic vector. Gene *108*, 193–199. https://doi.org/10.1016/0378-1119(91)90434-d.

59. Liew, C.G., Draper, J.S., Walsh, J., Moore, H., and Andrews, P.W. (2007). Transient and stable transgene expression in human embryonic stem cells. Stem Cell. *25*, 1521–1528. https://doi.org/10.1634/stemcells.2006-0634.

60. Dorrell, M.I., Aguilar, E., Jacobson, R., Yanes, O., Gariano, R., Heckenlively, J., Banin, E., Ramirez, G.A., Gasmi, M., Bird, A., et al. (2009). Antioxidant or neurotrophic factor treatment preserves function in a mouse model of neovascularization-associated oxidative stress. J. Clin. Investig. *119*, 611–623. https://doi.org/10.1172/jci35977.

61. Wu, K.H.C., Madigan, M.C., Billson, F.A., and Penfold, P.L. (2003). Differential expression of GFAP in early v late AMD: a quantitative analysis. Br. J. Ophthalmol. *87*, 1159–1166. https://doi.org/10.1136/bjo.87.9.1159.

62. Bringmann, A., Iandiev, I., Pannicke, T., Wurm, A., Hollborn, M., Wiedemann, P., Osborne, N.N., and Reichenbach, A. (2009). Cellular signaling and factors involved in Müller cell gliosis: neuroprotective and detrimental effects. Prog. Retin. Eye Res. *28*, 423–451. https://doi.org/10.1016/j.preteyeres.2009.07.001.

63. Reichenbach, A., Wurm, A., Pannicke, T., Iandiev, I., Wiedemann, P., and Bringmann, A. (2007). Müller cells as players in retinal degeneration and edema. Graefes Arch. Clin. Exp. Ophthalmol. *245*, 627–636. https://doi.org/10.1007/s00417-006-0516-y.

64. Canto, A., Martínez-González, J., Miranda, M., Olivar, T., Almansa, I., and Hernández-Rabaza, V. (2022). Sulforaphane Modulates the Inflammation and Delays Neurodegeneration on a Retinitis Pigmentosa Mice Model. Front. Pharmacol. *13*, 811257. https://doi.org/10.3389/fphar.2022.811257.

65. Hippert, C., Graca, A.B., Barber, A.C., West, E.L., Smith, A.J., Ali, R.R., and Pearson, R.A. (2015). Müller glia activation in response to inherited retinal degeneration is highly varied and disease-specific. PLoS One *10*, e0120415. https://doi.org/10.1371/journal.pone.0120415.

66. Fenner, B.J., Tan, T.E., Barathi, A.V., Tun, S.B.B., Yeo, S.W., Tsai, A.S.H., Lee, S.Y., Cheung, C.M.G., Chan, C.M., Mehta, J.S., and Teo, K.Y.C. (2021). Gene-Based Therapeutics for Inherited Retinal Diseases. Front. Genet. *12*, 794805. https://doi.org/10.3389/fgene.2021.794805.

67. Drag, S., Dotiwala, F., and Upadhyay, A.K. (2023). Gene Therapy for Retinal Degenerative Diseases: Progress, Challenges, and Future Directions. Investig. Ophthalmol. Vis. Sci. *64*, 39. https://doi.org/10.1167/iovs.64.7.39.

68. Chew, L.A., and Iannaccone, A. (2023). Gene-agnostic approaches to treating inherited retinal degenerations. Front. Cell Dev. Biol. *11*, 1177838. https://doi.org/10.3389/fcell.2023.1177838.

69. John, M.C., Quinn, J., Hu, M.L., Cehajic-Kapetanovic, J., and Xue, K. (2022). Gene-agnostic therapeutic approaches for inherited retinal degenerations. Front. Mol. Neurosci. *15*, 1068185. https://doi.org/10.3389/fnmol.2022.1068185.

70. Cehajic-Kapetanovic, J., Singh, M.S., Zrenner, E., and MacLaren, R.E. (2023). Bioengineering strategies for restoring vision. Nat. Biomed. Eng. *7*, 387–404. https://doi.org/10.1038/s41551-021-00836-4.

71. Kaur, G., and Singh, N.K. (2023). Inflammation and retinal degenerative diseases. Neural Regen. Res. *18*, 513–518. https://doi.org/10.4103/1673-5374.350192.

72. Murakami, Y., Ishikawa, K., Nakao, S., and Sonoda, K.H. (2020). Innate immune response in retinal homeostasis and inflammatory disorders. Prog. Retin. Eye Res. *74*, 100778. https://doi.org/10.1016/j.preteyeres.2019.100778.

73. Okita, A., Murakami, Y., Shimokawa, S., Funatsu, J., Fujiwara, K., Nakatake, S., Koyanagi, Y., Akiyama, M., Takeda, A., Hisatomi, T., et al. (2020). Changes of Serum Inflammatory Molecules and Their Relationships with Visual Function in Retinitis Pigmentosa. Investig. Ophthalmol. Vis. Sci. *61*, 30. https://doi.org/10.1167/iovs.61.11.30.

74. Veleri, S., Lazar, C.H., Chang, B., Sieving, P.A., Banin, E., and Swaroop, A. (2015). Biology and therapy of inherited retinal degenerative disease: insights from mouse models. Dis. Model. Mech. *8*, 109–129. https://doi.org/10.1242/dmm.017913.

75. Santos, A., Humayun, M.S., de Juan, E., Jr., Greenburg, R.J., Marsh, M.J., Klock, I.B., and Milam, A.H. (1997). Preservation of the inner retina in retinitis pigmentosa. A morphometric analysis. Arch. Ophthalmol. *115*, 511–515. https://doi.org/10.1001/archopht.1997.01100150513011.

76. Ayton, L.N., Barnes, N., Dagnelie, G., Fujikado, T., Goetz, G., Hornig, R., Jones, B. W., Muqit, M.M.K., Rathbun, D.L., Stingl, K., et al. (2020). An update on retinal prostheses. Clin. Neurophysiol. *131*, 1383–1398. https://doi.org/10.1016/j.clinph.2019.11.029.

77. Wang, M., Ma, W., Zhao, L., Fariss, R.N., and Wong, W.T. (2011). Adaptive Müller cell responses to microglial activation mediate neuroprotection and coordinate inflammation in the retina. J. Neuroinflammation *8*, 173. https://doi.org/10.1186/1742-2094-8-173.

78. Devoldere, J., Peynshaert, K., De Smedt, S.C., and Remaut, K. (2019). Müller cells as a target for retinal therapy. Drug Discov. Today *24*, 1483–1498. https://doi.org/10.1016/j.drudis.2019.01.023.

79. Xia, X., and Ahmad, I. (2016). Unlocking the Neurogenic Potential of Mammalian Müller Glia. Int. J. Stem Cells *9*, 169–175. https://doi.org/10.15283/ijsc16020.

80. Ross, M., and Ofri, R. (2021). The future of retinal gene therapy: evolving from subretinal to intravitreal vector delivery. Neural Regen. Res. *16*, 1751–1759. https://doi.org/10.4103/1673-5374.306063.

81. Mates, L., Chuah, M.K., Belay, E., Jerchow, B., Manoj, N., Acosta-Sanchez, A., Grzela, D.P., Schmitt, A., Becker, K., Matrai, J., et al. (2009). Molecular evolution of a novel hyperactive Sleeping Beauty transposase enables robust stable gene transfer in vertebrates. Nat. Genet. *41*, 753–761. https://doi.org/10.1038/ng.343.

82. Bartoletti, D.C., Harrison, G.I., and Weaver, J.C. (1989). The number of molecules taken up by electroporated cells: quantitative determination. FEBS Lett. *256*, 4–10. https://doi.org/10.1016/0014-5793(89)81707-7.

83. Vaessen, E.M.J., Timmermans, R.A.H., Tempelaars, M.H., Schutyser, M.A.I., and den Besten, H.M.W. (2019). Reversibility of membrane permeabilization upon pulsed electric field treatment in Lactobacillus plantarum WCFS1. Sci. Rep. *9*, 19990. https://doi.org/10.1038/s41598-019-56299-w.

84. Hoffmann, A., Bredno, J., Wendland, M., Derugin, N., Ohara, P., and Wintermark, M. (2011). High and Low Molecular Weight Fluorescein Isothiocyanate (FITC)-Dextrans to Assess Blood-Brain Barrier Disruption: Technical Considerations. Transl. Stroke Res. *2*, 106–111. https://doi.org/10.1007/s12975-010-0049-x.

85. Yumura, S., Matsuzaki, R., and Kitanishi-Yumura, T. (1995). Introduction of macromolecules into living Dictyostelium cells by electroporation. Cell Struct. Funct. *20*, 185–190. https://doi.org/10.1247/csf.20.185.